The Thesis committee for Niveditha Hanumantha Reddy
Certifies that this is the approved version of the following thesis:

A Procedure to Predict the Energy Harvest of Photovoltaic Arrays using only Global Horizontal Radiation Measurements

APPROVED BY
SUPERVISING COMMITTEE:

Supervisor:

W. Mack Grady

Surya Santoso

A Procedure to Predict the Energy Harvest of Photovoltaic Arrays using only Global Horizontal Radiation Measurements

by

Niveditha Hanumantha Reddy, B.E

Thesis

Presented to the Faculty of the Graduate School

of The University of Texas at Austin

in Partial Fulfillment

of the Requirements

for the Degree of

Master of Science in Engineering

The University of Texas at Austin

May, 2010

Dedication

This thesis is dedicated to my family - my source of unconditional love and support.

Acknowledgements

I consider it my privilege to express a few words of gratitude and respect to all those who guided and encouraged me during my work on this thesis.

I am highly indebted to my advisor, Dr. W. Mack Grady for his invaluable guidance and support. Working under him, as his research assistant, has been an incredible learning experience.

I am grateful to my friends Archana Sastry, Bhargavi Devarajan, Harini Janakiraman, Puja Kowley and Saloni Naik for providing me with the moral support required to successfully complete work on this thesis.

May, 2010

Abstract

A Procedure to Predict the Energy Harvest of Photovoltaic Arrays using only Global Horizontal Radiation Measurements

by

Niveditha Hanumantha Reddy, MSE

The University of Texas at Austin, 2010

SUPERVISOR: W. Mack Grady

This thesis uses the results of analysis of data recorded at a solar monitoring station in West Texas and the knowledge from an existing solar radiation estimation model to develop a methodology to predict the energy output from a panel at a site using only partial radiation data - global horizontal radiation measurements. The prediction using partial data is validated against estimates acquired using the complete radiation data and constraints are defined for accurate prediction. The methodology presented in this thesis can be used to accurately predict the solar power/energy incident on a collector at any location possessing global horizontal radiation measurements.

Table of Contents

List of Tables

List of Figures

Chapter 1

Introduction

In 15 minutes, the sun emits as much energy as mankind consumes in all forms, during an entire year. The energy radiated by the sun in a day is enough to power the entire United States for a year and a half [1]. If just 0.2% of the energy incident on the nation were converted to usable energy, the energy demand of the entire country could be met [2]. In addition, the fact that solar power is clean and renewable makes it an attractive source of energy for a multitude of applications. The most important among these are a) photovoltaics that convert sunlight directly to electricity b) solar thermal for industrial and household heating purposes c) solar thermal electric for producing steam to run turbines that generate electricity.

In addition to the dependence on the capital and operating costs, the economics of these technologies depend heavily on the amount of solar radiation that is available for conversion and the fraction of this available radiation that can be converted into heat or electricity. Designers and users of solar energy systems need high quality solar radiation data and energy output prediction methodologies in order to optimally size and achieve the performance and economic goals of the system.

Solar radiation data provides information regarding the amount of solar energy or power that strikes a surface, at any location on the earth. When recorded over a period of time, this data shows the variation in the quantity and intensity of the solar radiation received during that period at that location.

In order to determine the performance and economics of solar conversion technologies, designers use solar radiation data to estimate the quantity of solar energy available at the site. The three main solar radiation measurements used for the purpose of estimation are a) global radiation on a horizontal surface, b) diffuse radiation on a horizontal surface and c) direct normal/beam radiation measured normal to the rays.

Using all the three components for the purpose of prediction gives the most precise estimate. However, a variety of instrumentation is required to measure and record these components of solar radiation. Financial constraints may allow investment in instrumentation that can measure only one or two of the components.

This thesis uses data recorded at a solar monitoring station in West Texas to develop methodologies to predict the energy output from a panel at the site using only partial radiation data. The prediction using partial data is validated against estimates acquired using the complete radiation data.

Chapter 2 presents an existing model that can predict the solar radiation using as inputs only the geographical location of the site, day of the year and time of the day. The different solar radiation components and instrumentation used for solar radiation measurement are discussed in Chapter 3. Chapter 4 provides a brief insight into the working of the excel spreadsheet used for the analysis of the solar radiation data. The purpose of this thesis is explained in Chapter 5. Chapter 6 briefly describes the method for predicting the beam radiation using global and diffuse horizontal measurements. Chapter 7 explains the process of arriving at the methodology for predicting a) the beam radiation using only global horizontal measurements and b) the total incident power and energy on the panel. Finally, the model developed is validated and constraints are established for accurate prediction.

Chapter 2

Solar Radiation Estimation

In order to predict the availability of sunlight and the energy that can be harnessed from it, a fairly straightforward set of equations can be used. This section discusses the different parameters that are used in solar energy calculations [3]. An existing solar radiation prediction model [3] is presented.

2.1 Parameters of the solar resource

2.1.1 Air mass ratio

The intensity of the solar radiation striking the earth's surface depends on how much of the atmosphere the radiation has to pass through before reaching the surface. The air mass ratio m is a measure of this dependence.

$$Air\ mass\ ratio\ m = \frac{h_2}{h_1} = \frac{1}{\sin\beta} \tag{1}$$

where h_1= path length through the atmosphere with the sun directly overhead, h_2= path length through the atmosphere to reach a spot on the surface and β is the altitude angle of the sun. While an air mass ratio of 1 means the sun is directly overhead, a value of 0 means there's no atmosphere.

2.1.2 Solar declination angle

The angle between the plane of the equator and a line joining the center of the sun with the center of the earth is the solar declination angle, δ. It is a function of the day of the year and varies between +/- 23.45^0.

$$\delta = 23.45 \sin\left[\frac{360}{365}(n - 81)\right] \tag{2}$$

2.1.3 Hour angle

The hour angle, H is the number of degrees that the earth must rotate before the sun will be directly over the local longitude.

$$Hour\ Angle\ H = \left(\frac{15^0}{hour}\right) \times (hours\ before\ solar\ noon) \tag{3}$$

2.1.4 Solar altitude angle and azimuth angles:

These two angles, which depend on the latitude, day number and time of day, describe the position of the sun at any time of the day. The solar altitude angle: the angle between the sun and the horizon directly beneath the sun is denoted by β.

$$\sin\beta = \cos L\ \cos\delta \cos H + \sin L\ \sin\delta \tag{4}$$

where L denotes the latitude.

The solar zenith angle, θ_z is the angle complementary to the altitude angle. It is the angle between the sun and the axis drawn directly overhead at a site.

$$\theta_z = 90^0 - \beta \tag{5}$$

The solar azimuth angle φ_s is positive in the morning with the sun in the east and negative in the afternoon with the sun in the west if true south is used as reference.

$$\sin\varphi_s = \frac{\cos\delta\ \sin H}{\cos\beta} \tag{6}$$

2.1.5 Radiation on a collector surface:

Radiation striking the surface of a collector is a combination of direct-beam radiation, diffuse radiation and reflected radiation. While concentrating collectors which use focusing devices use only the direct-beam portion, most other photovoltaic systems which do not use focusing devices use all the three components.

The beam portion of radiation reaching the earth's surface normal to the rays, denoted by I_B is given by

$$I_{B=}Ae^{-km} \tag{7}$$

where A is the apparent extraterrestrial flux multiplier, k is a dimensionless factor called the optical depth and m is the air mass ratio. A and k are both sinusoidal functions of the day number n.

$$A = 1160 + 75 \sin\left[\frac{360}{365}(n - 275)\right] (W|m^2) \tag{8}$$

$$k = 0.174 + 0.035 \sin\left[\frac{360}{365}(n - 100)\right] \tag{9}$$

2.2 Model to predict total clear sky insolation on a panel

2.2.1 Direct-beam radiation

This radiation comes in a direct line from the sun. On clear days, most of the radiation is direct beam. Direct-beam radiation I_B striking the face of the collector, denoted at I_{BC} is given by

$$I_{BC} = I_B \cos\theta \tag{10}$$

where θ, the angle of incidence is the angle between the line drawn perpendicular to the face of the collector and the incoming beam.

$$\cos\theta = \cos\beta \cos(\varphi_s - \varphi_c) \sin\Sigma + \sin\beta \cos\Sigma \tag{11}$$

where φ_c is the collector azimuth angle and Σ is the collector tilt angle.

Beam insolation on a horizontal surface I_{BH},

$$I_{BH} = I_B \sin\beta \tag{12}$$

2.2.2 Diffuse radiation

Diffuse radiation consists of rays that are scattered out of the direct beam by molecules, aerosols and clouds. The fraction of total solar radiation that is diffuse is about 10% to 20% for clear skies and up to 100% for cloudy days [3]. Diffuse radiation on a horizontal surface,

$$I_{DH} = CI_B \tag{13}$$

where C, the sky diffuse factor is given by

$$C = 0.095 + 0.04 \sin\left[\frac{360}{365}(n - 100)\right] \tag{14}$$

If Σ is the panel tilt angle, diffuse radiation on the collector,

$$I_{DC} = CI_B\left(\frac{1+\cos\Sigma}{2}\right) \tag{15}$$

2.2.3 Reflected radiation

Insolation striking a collector surface after reflecting off surfaces around the panel constitutes reflected radiation. While no reflected radiation strikes a horizontal surface, the reflected radiation on panels tilted at Σ is given by:

$$I_{RC} = \rho(I_{BH} + I_{DH})\left(\frac{1-\cos\Sigma}{2}\right) \tag{16}$$

where ρ is the ground reflectance.

2.2.4 Total radiation on a horizontal collector

$$I_{CH} = I_{BH} + I_{DH} \tag{17}$$

2.2.5 Total radiation on a tilted collector

$$I_C = I_{BC} + I_{DC} + I_{RC} \tag{18}$$

Chapter 3

Solar Radiation Measurements

In order to study the performance of the solar collector, the three main solar radiation measurements that are used are [4]:

1) Global Horizontal (GH): It is the total solar radiation from the entire sky; the sum of the direct-beam, diffuse and reflected solar radiation. It is a different terminology used for I_{CH} calculated using (17).

2) Diffuse Horizontal (DH): It is the radiation from the entire sky excluding the sun disk. In the absence of an atmosphere, this component of radiation would not exist. This refers to I_{DH} calculated using (13).

3) Direct Normal (DN): It is the solar radiation from the direction of the sun. This refers to I_B calculated using (7).

3.1 Solar radiation measurement instrumentation:

3.1.1 Pyranometer:

While a pyranometer with a 180^0 view measures global solar radiation, one with a shadow band is used to measure diffuse solar radiation. The shadow band serves to block out the direct beam radiation so that the pyranometer sees only the diffuse radiation. Pyranometers are commonly used for solar energy studies. They are mounted horizontally at meteorological stations, and on solar panels, with the sensor surface in the plane of the panel [4].

3.1.2 Pyrheliometer:

A pyrheliometer is an instrument with a narrow field of view used for the measurement of direct normal irradiance. It is mounted onto a solar tracking system in order to keep the instrument aimed at the sun. It is very often used along with a pyranometer. It is an expensive purchase since a solar tracker is an added expense.

3.1.3 Spectroradiometer:

A spectroradiometer measures the spectral distribution of solar radiation.

3.1.4 Rotating shadow band radiometer at Saragosa, Texas:

The solar radiation measurement instrumentation used to record the data at Saragosa, Texas, that was used for this thesis is the rotating shadow band radiometer. This instrument is used to measure both global and diffuse solar radiation. A motor is used to move the shadow band. When the shadow band shades the sensor, diffuse radiation is measured. The motor then unshades the sensor so that it can measure the global radiation.

3.2 Solar Radiation Measurement Instrumentation at The University of Texas at Austin

A Sci Tek 2AP tracker installed at UT Austin takes GH, DH and DN readings every five minutes using three separate thermo-couple sensors. While the DN sensor (pyrheliometer) tracks the sun and measures the beam radiation, the GH sensor (180^0 view pyranometer) points straight up and measures the radiation from the entire sky. The DH sensor (shaded pyranometer) also points straight up, but in order to block out the radiation from the sun disk, a shadow ball is used. A rotating shadow band radiometer also records GH and DH values at this location.

Chapter 4

The Solar Analyzer

The solar analyzer is an Excel Spreadsheet developed by Dr. Mack Grady for the purpose of analyzing solar radiation data. It consists of a module with a variety of features encoded in Visual Basic. This section elaborates on the functionality of those existing features that are used for the purpose of this thesis. New additions made to the spreadsheet to aid in data analysis will be described in the next chapter. All the graphs included in this chapter are plotted with the local clock time along the x-axis.

Data comprising the following components is recorded at five minute intervals by solar radiation measurement apparatus at Saragosa, Texas:

- Time of recording
- Measured Global Horizontal Radiation (W/ m^2)
- Measured Diffuse Horizontal Radiation (W/ m^2)
- Global Radiation on panel array measured using a Li-Cor sensor (W/ m^2)
- Global Horizontal Radiation measured using a Li-Cor sensor (W/ m^2)

Table 1 shows a sample recording at 7:00 am clock time on January 1, 2009 at Saragosa.

Hour_Min	Measured GH (W/ m^2)	Measured DH (W/ m^2)	Measured Li-Cor_PanelArray (W/ m^2)	Measured Li-Cor_GH (W/ m^2)
700	61	59.8	65.7	67.8

Table 1: Measured Solar radiation data on January 1, 2009 at Saragosa, Texas

Data is recorded into a *dat* file. The Excel Solar Analyzer uses these *dat* files as input and loads the data into the excel spreadsheet for analysis. Figure 1 is a screenshot of the portion of the form/user-interface (UI) developed in Visual Basic that was used for this thesis. On specifying the path to the *dat* file (in this case Saragosa_1.dat) and

selecting the 'Read Data File' button, the data file is read. Based on the day selected in the 'Single Day Analysis' section, the program fetches the data corresponding to that day from the *dat* file and populates cells in the spreadsheet with it. In order to allow the user to verify the content of the data file extracted, the UI displays the first and last two lines read from the data file.

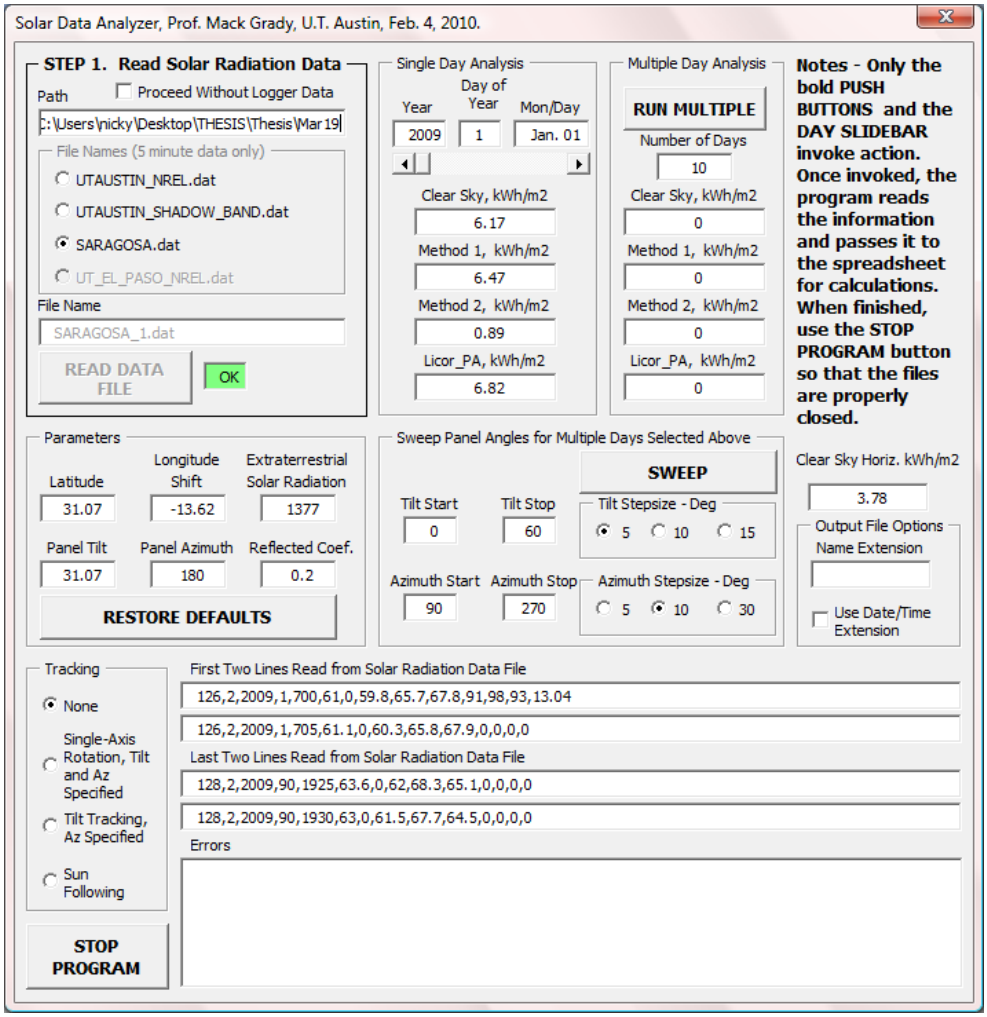

Fig.1: Portion of User-interface of Excel Solar Analyzer used.

Once the spreadsheet is populated with the data, it performs a number of operations such as the calculation of zenith, altitude, azimuth and incident angles, air mass ratio, extra-terrestrial flux multiplier, optical depth, beam reaching the earth's

surface, sky diffuse factor etc, which will all be used in the estimation of solar radiation on the panel.

The form takes as inputs parameters such as latitude, longitude shift, extra-terrestrial solar radiation, panel tilt and azimuth angles and reflectance coefficient values. A method of solar tracking among the following needs to be selected: a) None, b) Single axis rotation with panel tilt and azimuth angles specified, c) Tilt tracking with azimuth angle specified or d) Sun following with neither panel tilt not azimuth angle specified.

The 'Single Day Analysis' section allows the user to pick a day for which the data analysis needs to be performed. Using the data extracted into it and results of calculations performed by it, the spreadsheet uses four different methods to calculate the solar radiation on the panel.

1) Clear Sky: This method uses the model presented in Chapter 2 to estimate the solar radiation on the panel under clear sky conditions.

2) Method 1: This method utilizes the GH and DH values to estimate the solar radiation.

3) Method 2: This method uses the GH, DH and DN values to estimate solar insolation on the panel.

4) Licor_PA/Method 3: This method sums up the measured Li-Cor_PanelArray values for the day.

Methods 1 and 2 can be applied to GH, DH and DN values recorded by the instrumentation at UT-Austin to estimate solar radiation. Method 1 can be used to estimate solar radiation using the GH and DH values recorded by the rotating shadow-band radiomenter at Saragosa. The results in kWh/m^2, of the four estimations listed above, are displayed in the UI. The result obtained using Method 2 is significantly lower than that using the other methods since this method uses DN which is not recorded at Saragosa. For the purpose of calculation, Method 2 assumes DN to be zero.

For the purpose of this thesis, the inputs corresponding to location Saragosa were entered and tracking was selected as 'None'. The UI shows the results of single day analysis performed for January 1, 2009.

The module also provides the option to perform the estimations for multiple days at a time. Post-estimation, the UI displays the sum of the kWh/ m^2 for the multiple days for which the analysis was performed.

In addition, when sweep angles (panel tilt and azimuth angles) are specified, the program performs the estimations described above, for the specified number of days, for a range of specified angles and the results are recorded into a *csv* file. These results can be studied and plotted to determine the optimum panel tilt and azimuth angle for the specified days, be it a week, month, season or year.

The results of the spreadsheet and program calculations are plotted by the analyzer in several graphs from which useful information can be gathered. Figures 2, 3 and 4 show the variation of different solar angles during the day, January 1, 2009, at Saragosa, while Figure 5 shows the variation of the incidence angle of solar radiation on a panel with tilt angle = 31.07^o and azimuth angle = 180^o at Saragosa. All the measurements from the data file corresponding January 1, 2009 are plotted a graph depicted in Figure 6. The results of solar radiation estimations using methods 1, 2 and 3 for January 1, 2009, are plotted onto a graph shown in Figure 7.

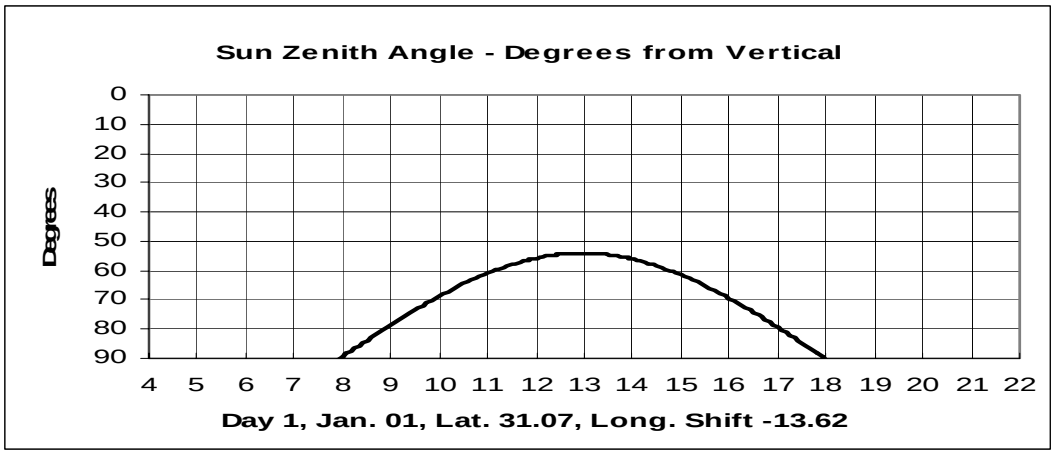

Fig. 2. Variation of solar zenith angle on January 1, 2009 at Saragosa

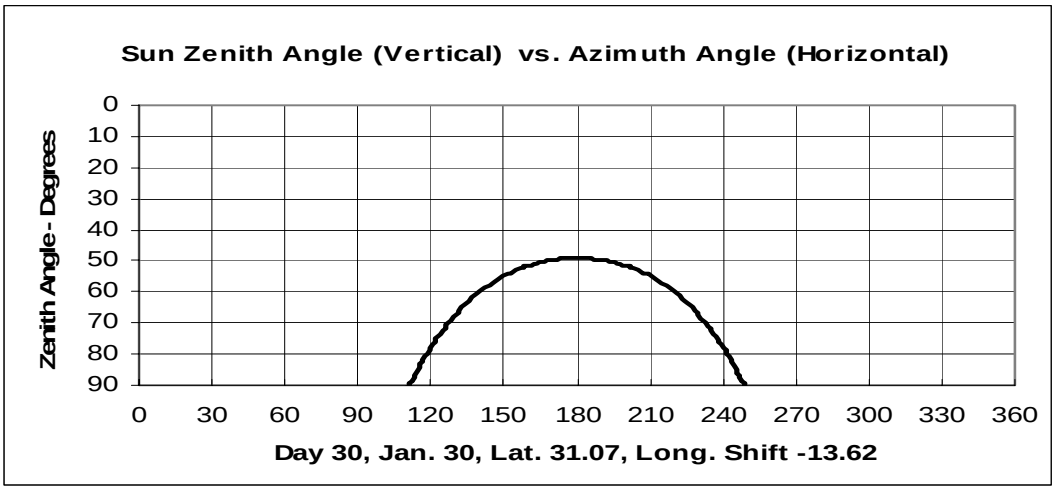

Fig.3. Variation of solar zenith angle versus solar azimuth angle on January 1, 2009 at Saragosa.

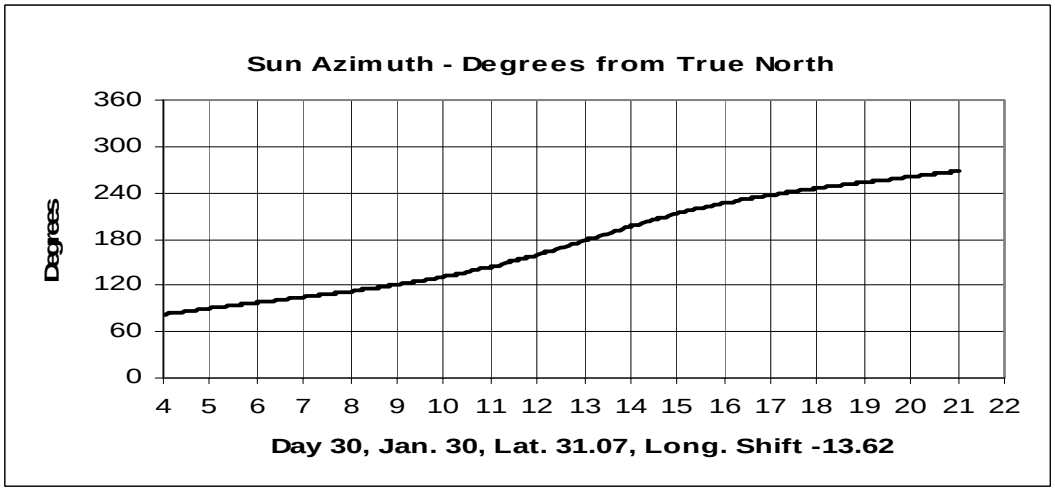

Fig.4. Variation of solar azimuth angle on January 1, 2009 at Saragosa

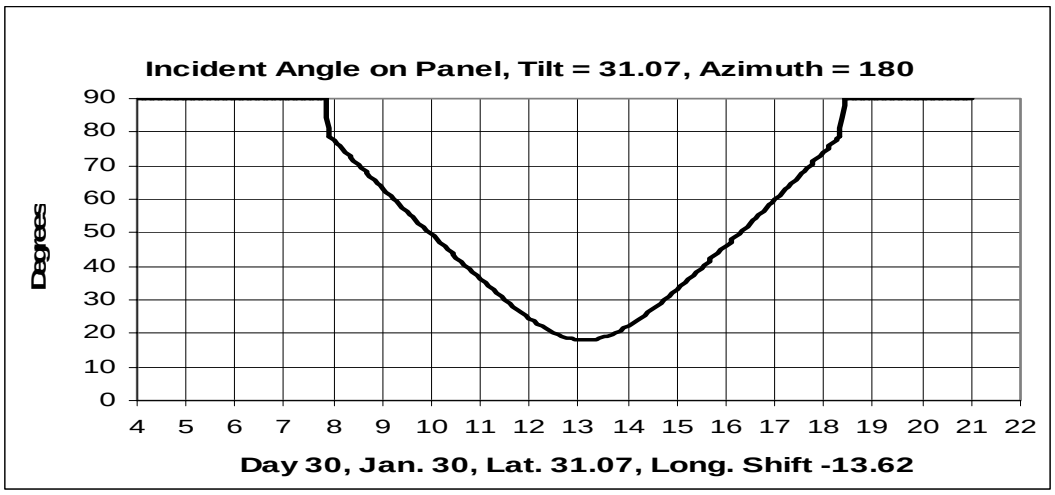

Fig.5. Variation of angle of incidence of solar radiation on panel

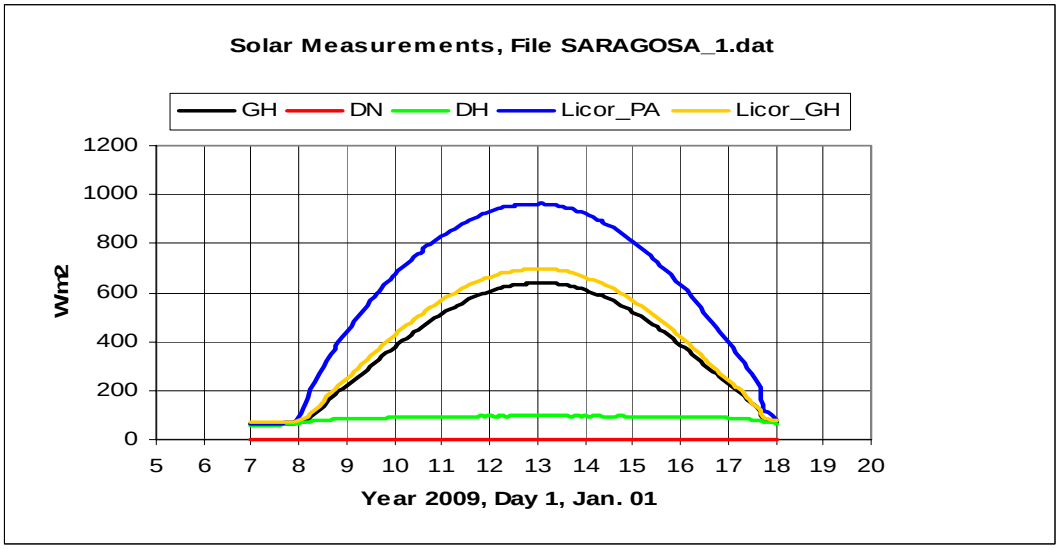

Fig.6. Plots of measurements of solar radiation components on January 1, 2009 at Saragosa

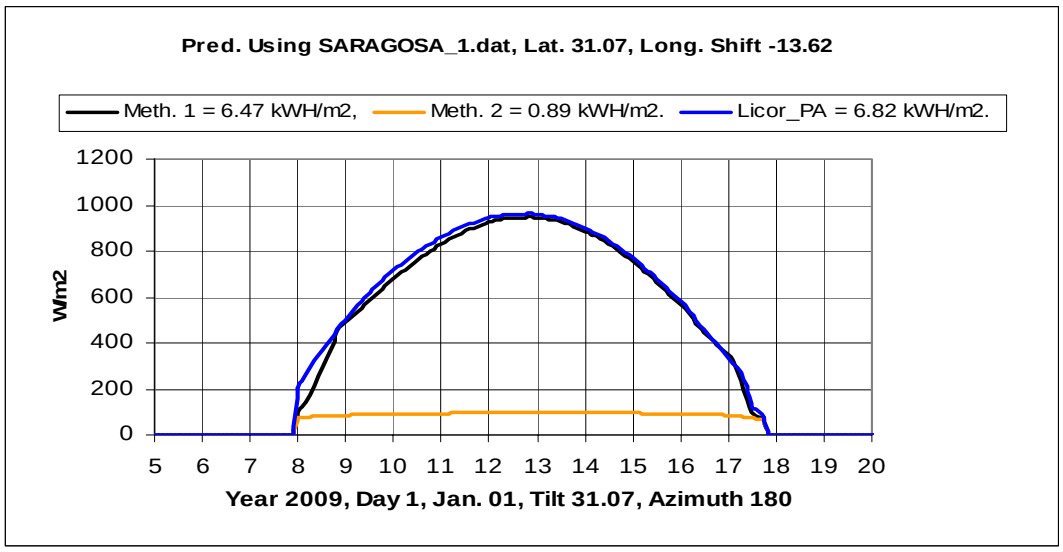

Fig.7. Estimated solar radiation at Saragosa on January 1, 2009 at Saragosa

Chapter 5

Prediction of Beam Radiation

Depending upon the kind of data that is required and the funding available, the number and kinds of solar data measurement instruments to be installed are determined. A solar monitoring station may have instrumentation to measure the three quantities: 1) Global radiation on a horizontal surface 2) Diffuse radiation on a horizontal surface, and 3) Direct beam (direct normal) radiation. Analysis using these three quantities provides sufficient insight into the solar resource and the potential for harvesting energy from it at any location.

Using any two of these quantities, a set of acceptable values of the third can be calculated. Therefore, in a station/establishment with funding constraints, instrumentation may be installed to measure only two quantities. The equation relating the three quantities is as follows [5]:

$$DN_{est} = DH + \frac{(GH - DH)}{\cos\theta_z} \tag{19}$$

The cosine term corrects for the fact that the GH sensor points straight up, but the radiation hits the sensor at an angle θ_z.

By substituting any two of the measured values into the equation, the third can be calculated. The trade-off for this approach is that the calculated values are less accurate than if the value were measured. The first part of this thesis uses the measured GH and DH values to calculate the DN values. These values are then compared with the measured DN values and the range of values of 1) θ_z and 2) DH_{meas}/GH_{meas} for which the calculated DN values match the measured values of DN is determined.

Many stations, especially those intended for agricultural use, measure only the global horizontal on a horizontal surface. The second part of this thesis focuses on using the measured GH values to predict the beam radiation on a horizontal surface, I_{BH} at a location. Firstly the plot of the measured GH curve is superimposed on the curve of

estimated I_{BH} plotted using I_{BH} values predicted using the model presented in Chapter 2. The behavior of these curves on each day during the year 2009 is analyzed. Based on certain observations made by analyzing the behavior of the curves, certain criteria are defined to indentify useful portions of data. These portions of data are accumulated into a single file and analyzed collectively. Using the results of the analysis, equations are developed to predict the I_{BH} values at a location. The methodology that can be used to calculate the parameters of these equations is presented so that the model developed can be employed to predict the I_{BH} at any location which records GH values. The procedure to predict the power incident on the collector using only measured GH and predicted IBH values is presented and validated.

Chapter 6

Prediction of Beam Radiation using Global and Diffuse Horizontal Measurements

The solar radiation measurement instrumentation at Saragosa, Texas, measure and record the global horizontal radiation (GH_{meas}), diffuse horizontal radiation (DH_{meas}), total radiation on a panel using a Li-Cor sensor (Li_PA) and global horizontal radiation using a Li-Cor sensor (Li_GH). This chapter discusses the attempt made to predict the beam radiation using both GH_{meas} and DH_{meas}

Using the model presented in Chapter 2, the beam radiation on a horizontal surface was predicted using the equation:

$$I_{BHpred} = I_B \sin\beta = I_B \cos\theta_z \tag{20}$$

Using the GH_{meas} and DH_{meas} values, the beam radiation on a horizontal panel, I_{BHmeas} was calculated using the equation:

$$I_{BHmeas} = GH_{meas} - DH_{meas} \tag{21}$$

The aim of the exercise was to determine a range of values of the following:

- DH_{meas}/GH_{meas}
- Solar zenith angle, θ_z

for which the I_{BHpred} is reasonably close to the I_{BHmeas} values.

Additional formulae were included in the spreadsheet to calculate the % deviation of I_{BHpred} from I_{BHmeas}. The analyzer program was run to identify the clear sky days from June to December 2009. On each of these days the I_{BHpred} and I_{BHmeas} were calculated and compared and the following graphs were plotted and analyzed:

- % deviation of I_{BHpred} from I_{BHmeas} vs. local clock time
- DH_{meas}/ GH_{meas} vs. local clock time
- Solar zenith angle, θ_z vs. local clock time

Figure 8 shows all the three plots, superimposed, for December 06, 2009, which was a clear sky day. From the figure, it can be observed that the deviation was 10% between 10am and 2pm. During this time period, the diffuse radiation accounted for 15% to 20% of the global horizontal radiation. Between the 9am to 4pm period, when the diffuse radiation accounted for 20% to 30% of the total radiation, the deviation was found to be less than 20%.

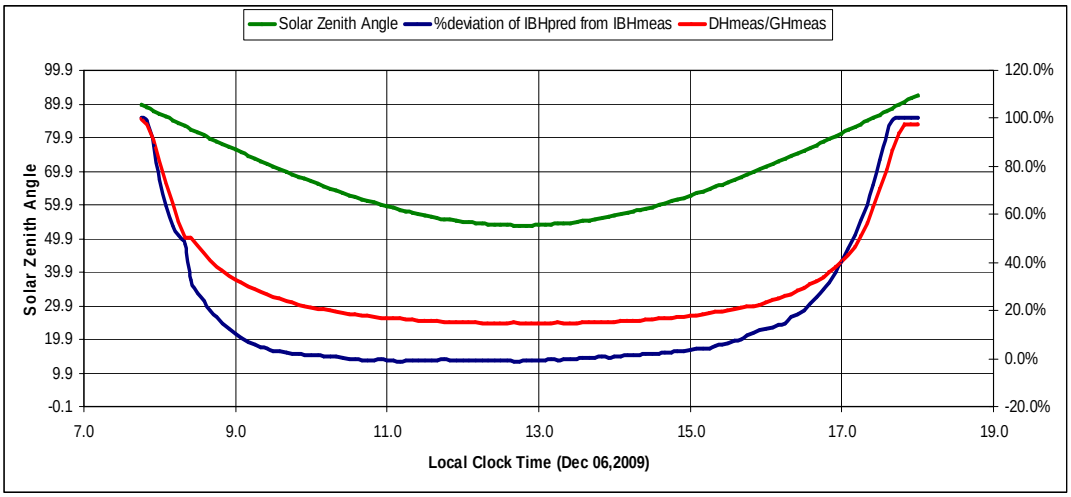

Fig.8. Variation of θ_z, % deviation of I_{BHpred} from I_{BHmeas} and DH_{meas}/GH_{meas} on December 06, 2009

Figure 9 shows the three plots for June 11, 2009, a day when the % deviation was higher than in the previous case. It can be observed from the graphs, that on this day, the % deviation was in the high 20% to 25% range between 10am and 4pm. During this time period, diffuse horizontal radiation formed a small fraction of the total radiation – only 7%.

Table 2 tabulates similar observations made for various clear sky days during the June to December, 2009 period. It was observed that generally, on clear sky days, the deviation of the predicted I_{BH} value was approximately less than 20% between 10am and 3pm. The % deviation was constant from June through December despite the fact that the zenith angle variation was considerable. Unexpectedly, on some days with very low DH component, the deviation was higher than on days with high DH.

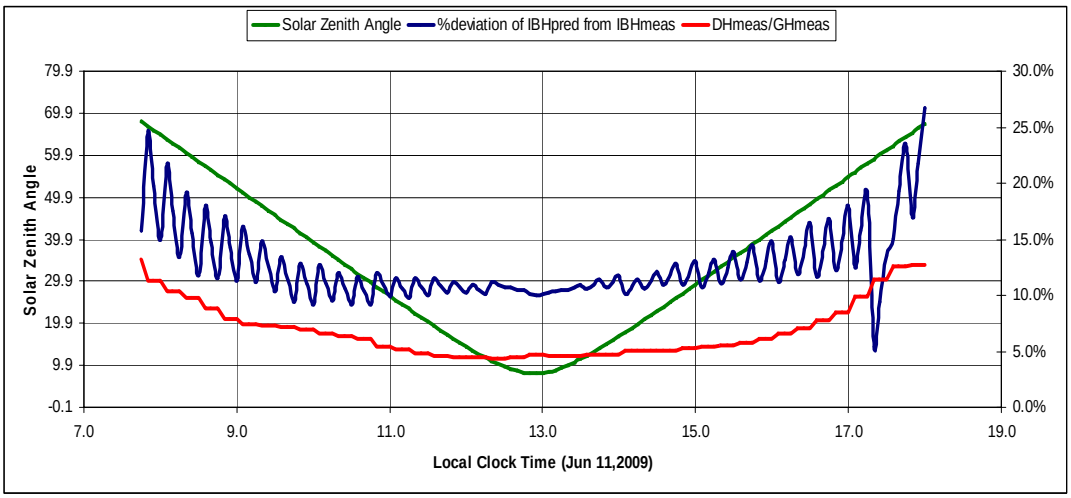

Fig.9. Variation of θ_z, % deviation of I_{BHpred} from I_{BHmeas} and DH_{meas}/GH_{meas} on June 11, 2009

Date (2009)	**% Deviation of I_{BHpred} from I_{BHmeas}**	**Corresponding Solar Zenith Angle range**	**Corresponding DHmeas/GHmeas**
11-Jun	In the 20 to 25% range between 10am and 4pm	39^o to 44^o	<7%
3-Jul	Around 20% between 10am and 4pm	$< 40^o$	<10%
25-Jul	<10% all day	for all values of zenith angle (0^o to 68^o)	ranged between 15% and 35%
26-Aug	<15% all day	for all values of zenith angle (0^o to 70^o)	ranged between 15% and 35%
1-Sep	<10% between 10am and 4pm,	for values of zenith angle (0^o to 72^o)	<20%
	<20% rest of the day		<30%
25-Sep	<10% between 9am and 3pm	for values of zenith angle between 45^o and 63^o	between 10% and 20%
29-Sep	<10% between 8am and 4pm	for values of zenith angle $<70^o$	between 20% and 25%

Table 2: Observations about the accuracy of I_{BH} prediction and corresponding time of day, solar zenith angle and DH_{meas}/ GH_{meas} ratio

Date (2009)	**% Deviation of I_{BHpred} from I_{BHmeas}**	**Corresponding Solar Zenith Angle range**	**Corresponding DHmeas/GHmeas**
15-Oct	in the 10% and 20% range between 9am and 4pm	for values of zenith angle $<70^o$	between 15% and 25%
4-Nov	in the 10% and 20% range between 9am and 4pm	for values of zenith angle $<70^o$	between 15% and 20%
11-Nov	<10% between 9am and 3pm,	for values of zenith angle $<65^o$	between 20% and 30%
22-Nov	<10% between 10am and 2pm,	for various values of zenith angle $<70^o$	between 15% and 20%
	<20% between 8am and 4pm		between 20% and 30%
6-Dec	<10% between 10am and 2pm,	deviation <10% for zenith angles $<65^o$	between 15% and 20%
	<20% between 9am and 4pm		between 20% and 30%
17-Dec	<10% between 9am and 3pm,	for various values of zenith angle $<70^o$	between 15% and 25%
	<20% between 9am and 4pm		between 20% and 30%

Table 2 (contd.): Observations about the accuracy of I_{BH} prediction and corresponding time of day, solar zenith angle and DH_{meas}/ GH_{meas} ratio

Chapter 7

Prediction of Beam Radiation and Energy Harvest using only Global Horizontal Measurements

This chapter discusses the methodology developed to predict a) the beam radiation on the collector using both GH_{meas} and DH_{meas} and b) the incident solar power on the collector.

The following graphs were plotted in the spreadsheet, with local clock time as the x-axis

Graph 1:

- Predicted total radiation on the collector, I_{Cpred}

  where

$$I_{Cpred} = I_{BCpred} + I_{DCpred} + I_{RCpred} \quad (22)$$

  I_{BCpred}, I_{DCpred} and I_{RCpred} are calculated using (10), (15) and (16) respectively.
- Global radiation on the panel array measured by the Li-Cor sensor, Li_PA
- Measured global horizontal values, GH_{meas}

Graph 2:

- Predicted beam radiation on horizontal surface, I_{BHpred}
- Measured global horizontal values, GH_{meas}

All the graphs included in this chapter (except the graph in Figure 23) are plotted with the local clock time along the x-axis. Figures 10 and 11 pertain to graphs 1 and 2 respectively, plotted for January 1, 2009 which was a clear sky day. By studying both the figures it can be observed that the GH_{meas} curve closely follows the I_{BHpred} curve.

Figure 12 and 13 pertain to graphs 1 and 2 respectively, plotted for January 5, 2009 which was a cloudy day. From the two figures it can be observed that the GH_{meas} curve closely follows the Li_PA curve.

The graphs were observed for a number of clear sky and non-clear sky days. The observations could be generalized as follows:

1) On clear sky days, the GH_{meas} values match the I_{BHpred} values. However, they are different from the Li_PA values. On clear days, with high fraction of beam component, the orientation of the panel matters. Since the Li_PA sensor is mounted on to a tilted collector, the radiation measured by it is significantly different from that measured by a GH sensor on a horizontal surface.

2) On non-clear sky/cloudy days the GH_{meas} curve closely follows the Li_PA curve. Since on cloudy days the diffuse component is high and the beam component is negligible, the orientation of the sensor is not as important. Hence, the radiation measured by the GH sensor on a horizontal surface and that measured by the Li-Cor sensor mounted onto the panel are similar.

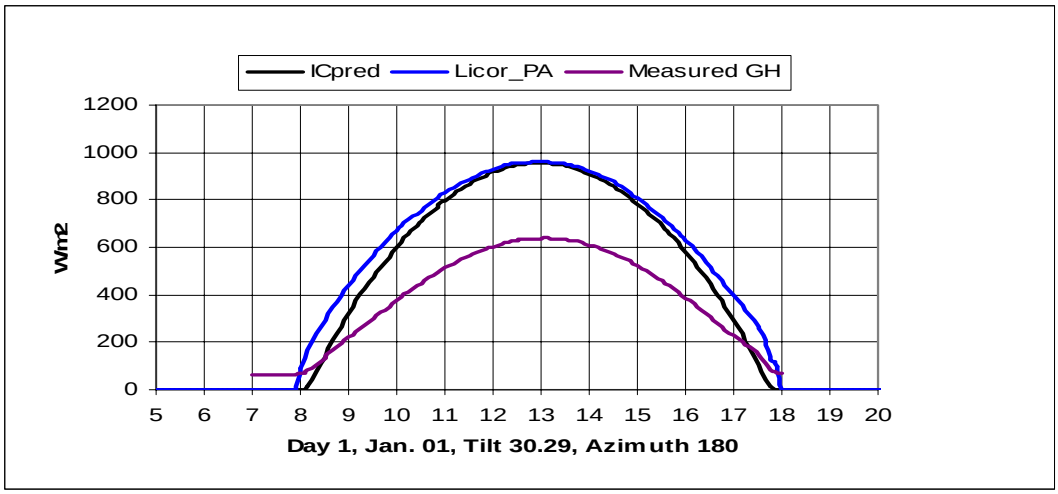

Fig.10. Plots of I_{Cpred}, Li_PA and GH_{meas} on a clear-sky day, January 1, 2009

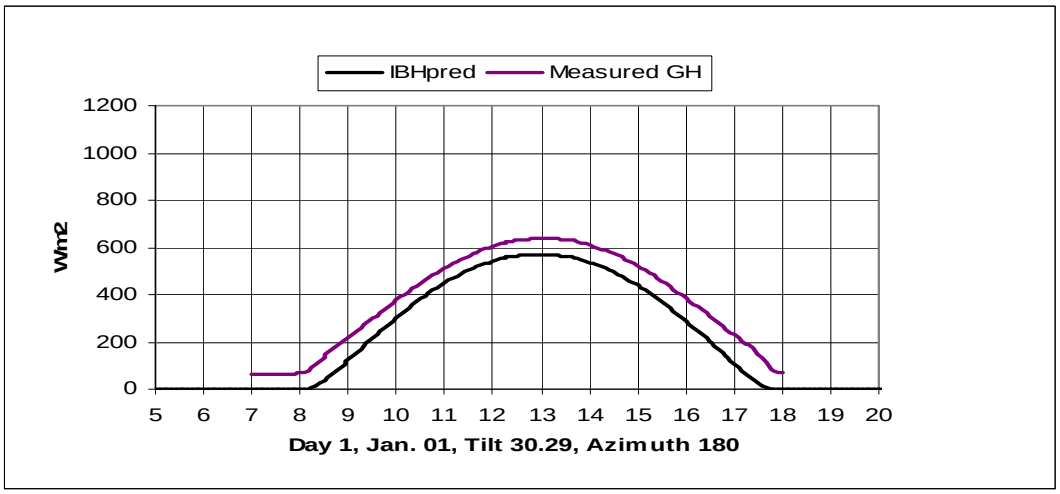

Fig.11. Plots of I_{BHpred} and GH_{meas} on a clear-sky day, January 1, 2009

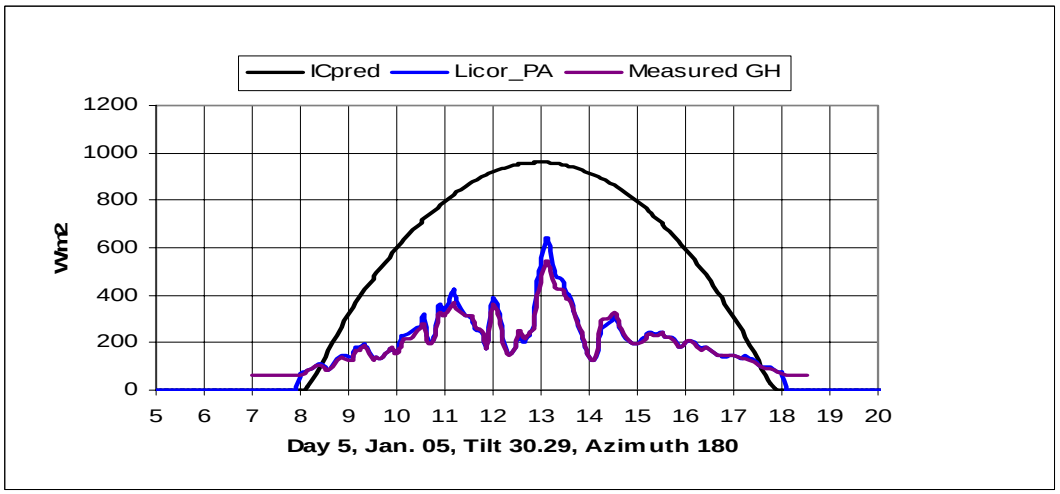

Fig.12. Plots of I_{Cpred}, Li_PA and GH_{meas} on a cloudy day, January 5, 2009

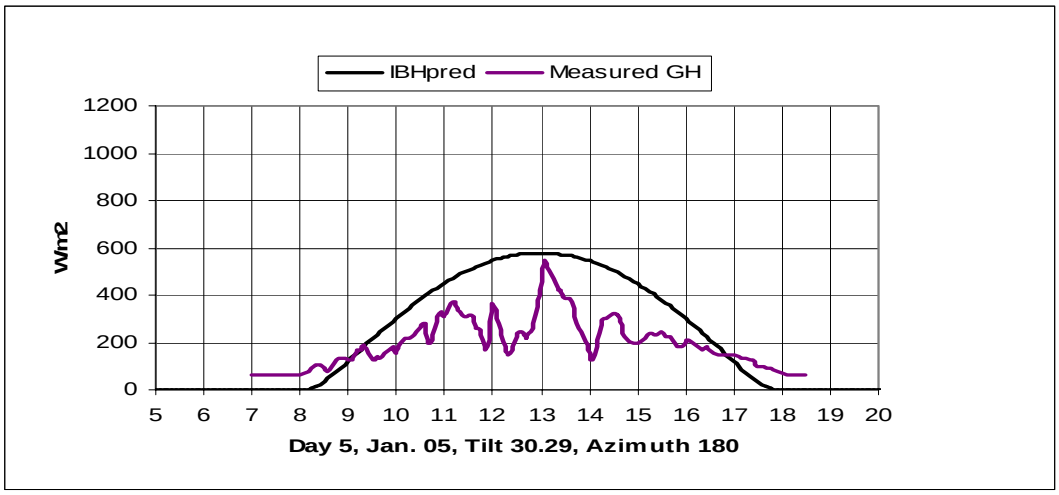

Fig.13. Plots of I_{BHpred} and GH_{meas} on a cloudy day, January 5, 2009

When the GH_{meas} curve lies below the I_{BHpred} curve, it indicates a cloudy day (for example, January 5, 2009) with solar radiation comprising mostly the diffuse component (Figure 13).

When the GH_{meas} curve lies above the I_{BHpred} curve (on clear sky days, for example the curves of January 1, 2009 in Figure 11), GH_{meas} is mostly composed of the beam component of radiation with negligible diffuse radiation component. Therefore, GH_{meas} curves on clear sky days were used to predict the beam radiation.

Before proceeding to the actual procedure to predict the beam radiation, the basic methodology is first outlined. I_{BHpred} was calculated using the equation:

$$I_{BHpred} = I_B \cos\theta_z \tag{23}$$

where

1) I_B, the beam portion of radiation reaching the earth's surface normal to the rays:

$$I_{B=}Ae^{-km} \tag{24}$$

2) A, the apparent extraterrestrial flux multiplier:

$$A = 1160 + 75\sin\left[\frac{360}{365}(n-275)\right](W|m^2) \tag{25}$$

3) k, a dimensionless factor called the optical depth:

$$k = 0.174 + 0.035 \sin\left[\frac{360}{365}(n - 100)\right] \tag{26}$$

4) m, the air mass ratio:

$$m = \frac{h_2}{h_1} = \frac{1}{\sin\beta} \tag{27}$$

In order to predict the beam radiation using the GH_{meas} plot, the curve underlying the plot needed to found. This could be achieved by varying the values of A and k in (24) in order to fit the I_{BHpred} to the GH_{meas} curve. Equations (25) and (26) are rewritten as follows:

$$A = B\left\{1 + C \sin\left[\frac{360}{365}(n - D)\right]\right\} \tag{28}$$

$$k = E\left\{1 + F \sin\left[\frac{360}{365}(n - G)\right]\right\} \tag{29}$$

By varying the values of B, C, D the value of A and by varying, E, F and G, the value of k could be varied respectively. Therefore, to find the curve underlying the GH_{meas} curve, (24) was modified by varying A and k, resulting in the variation of (23). The process is explained step-by-step below.

Step 1: Selection of Raw Data

In order to predict the beam radiation on a horizontal panel with maximum accuracy, it is necessary that numerous data points i.e, GH_{meas} values are used. Radiation data for the following days from the year 2009 at Saragosa was available for analysis:

- Days 1 to 90 – January 1 to March 31.
- Days 139 to 296 –May 19 to October 23
- Days 301 to 365 – October 28 to December 31

Data pertaining to all the above listed days was analyzed to pick out the days that were usable for the purpose of modeling the GH_{meas} curve.

Since solar radiation intensity is maximum at solar noon, and the yield from the panel is the highest around that time, only the 11am to 1pm solar time period was taken into consideration for analysis. Days with completely clear sky (days with smooth GH_{meas} curves in the 11am to 1pm period) during this time period were selected. In order to have all the useful data possible for the purpose of analysis, even days with the GH_{meas} curve that was smooth in parts were selected.

Firstly, the plots of GH_{meas} and I_{BHpred} vs. clock time of each day were studied. The screening process is explained below.

Figure 14 depicts a day with a perfectly smooth GH_{meas} curve. In particular, it is smooth in the 11am to 1pm solar time (or 12pm to 2pm clock time) region. One such day was selected.

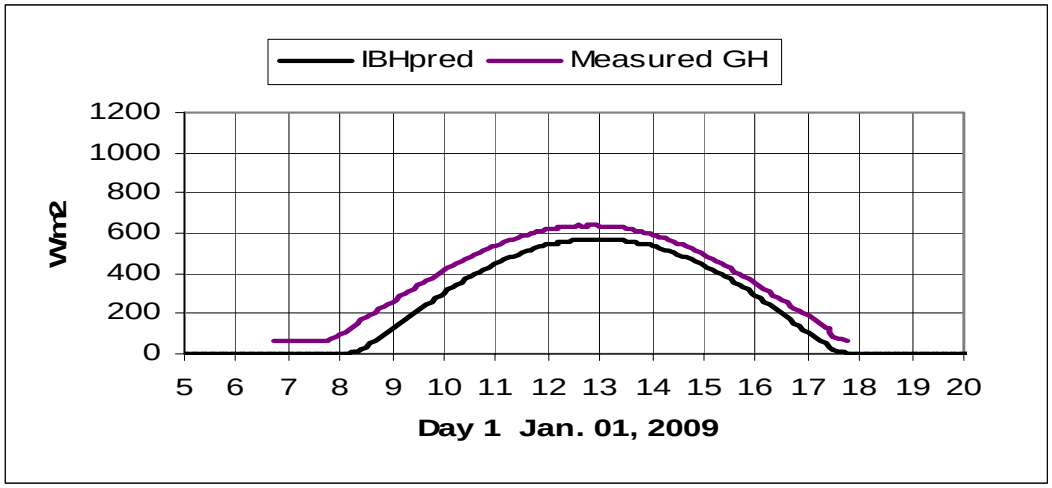

Fig.14. GH_{meas} curve that is smooth in the 11am to 1pm solar time period

Figure 15 depicts a day with a GH_{meas} curve that rises above the I_{BHpred} curve at different parts of the day but is not smooth, especially in the 11am to 1pm solar time period. Such a day, was omitted.

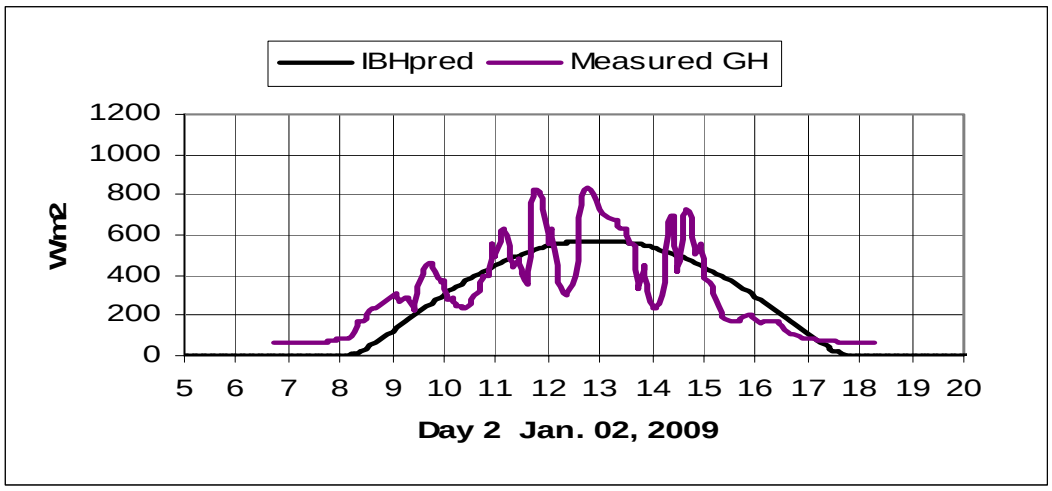

Fig.15. GH_{meas} curve that is varies sharply in the 11am to 1pm solar time period

Figure 16 depicts the GH_{meas} on a completely cloudy day. The GH_{meas} curve never surpasses the I_{BHpred} curve. Such a day, with a dominant DH component was not considered.

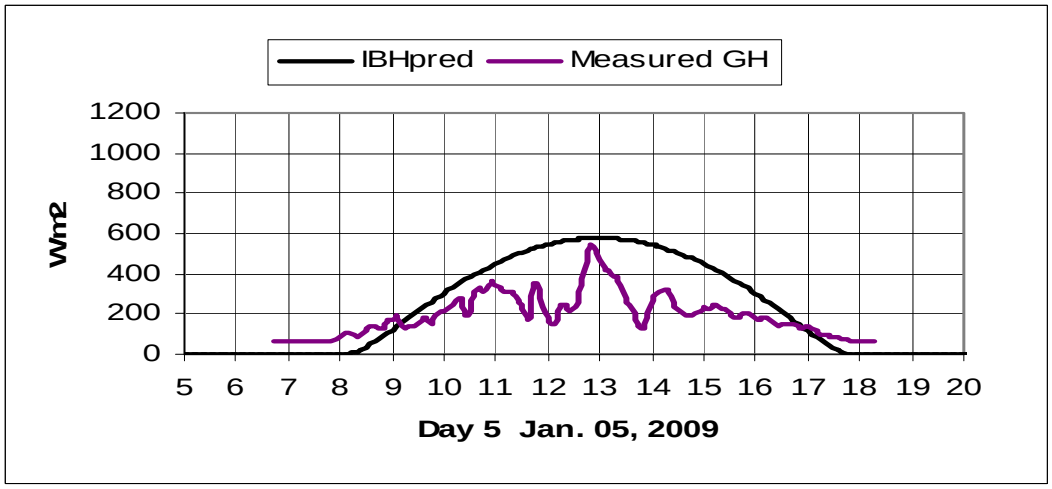

Fig.16. GH_{meas} curve that lies below the I_{BHpred} curve in the 11am to 1pm solar time period

Figure 17 depicts the GH_{meas} curve that is fairly smooth in the 11am to 1pm solar time period. Portions of this curve can be used for our analysis. Hence this day was chosen.

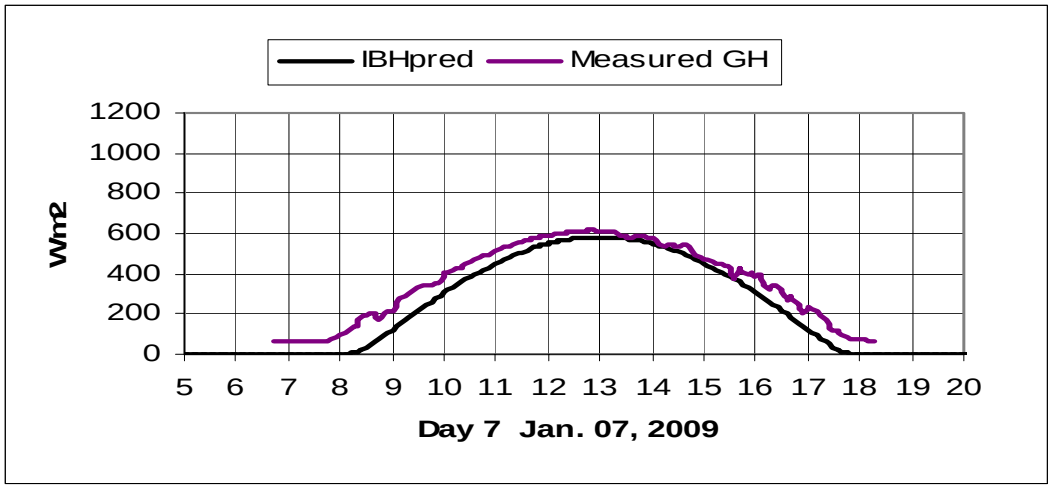

Fig.17. GH_{meas} curve that is fairly smooth in the 11am to 1pm solar time period

Step 2: Determination of curve underlying the GH_{meas} plot

In order to select usable portions of the GH_{meas} curves on the selected days, the following procedure was followed:

The I_{BHpred} curve was modified to fit the GH_{meas} curve. To achieve this, the least sum of squares method was used for curve fitting. In order to make the I_{BHpred} curve flexible, the value of extraterrestrial flux multiplier A used in the calculation of I_B was made variable. A was varied by varying the B, C and D values. A macro was written to run the excel solver that determined the optimum B,C and D values such that the resulting value of A fit the I_{BHpred} curve to the GH_{meas} curve minimizing the sum of squares of the differences between the GH_{meas} and I_{BHpred} curves.

Figure 18 shows the GH_{meas} curve before the I_{BHpred} curve was fitted to it. Figure 19 shows the I_{BHpred} curve fit to the GH_{meas} curve as a result of the macro execution. Before running the macro, the initial values of B, C and D were set to 1160, 0.0646 and 275 respectively. The solver determined the values of B, C and D to be 1148.2, 0.2315 and 336 respectively resulting in A=1301.76.

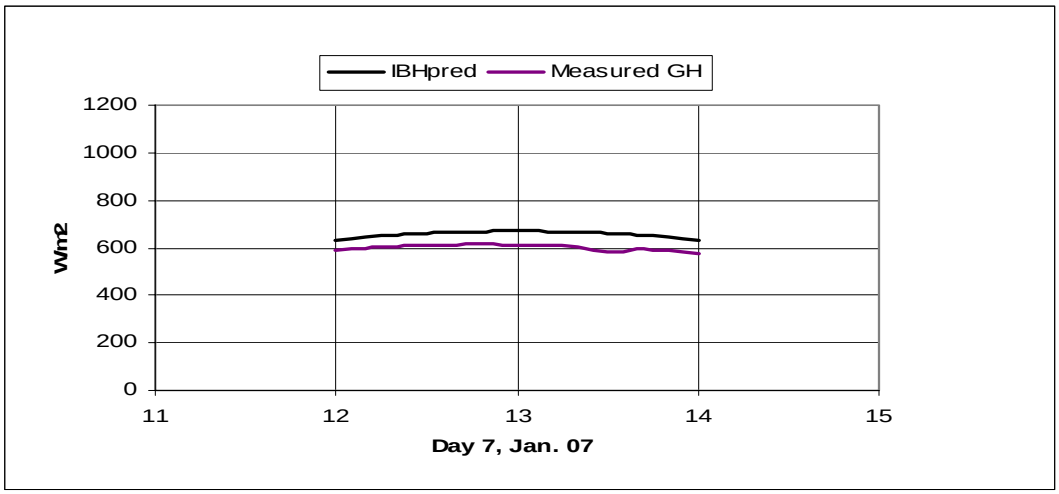

Fig.18. The I_{BHpred} curve prior to being curve fit to the GH_{meas} curve

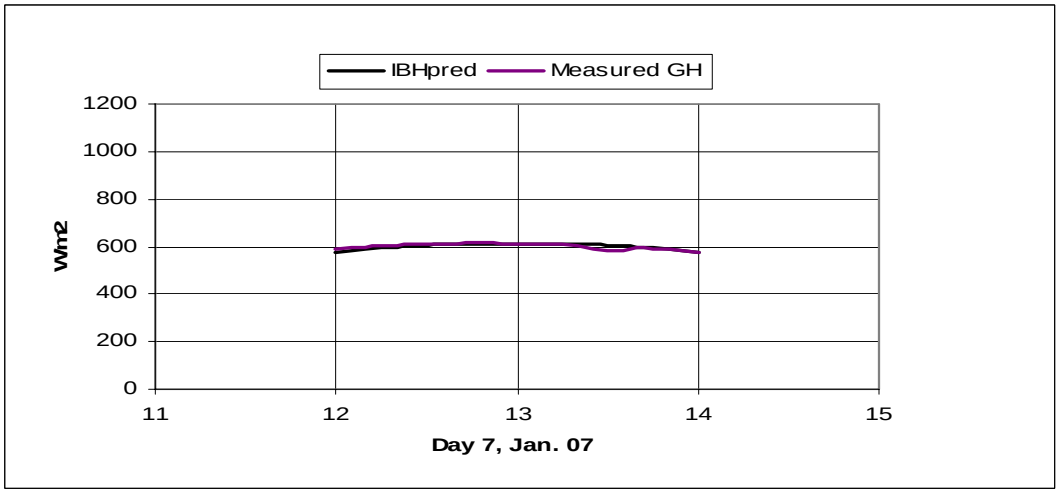

Fig.19. The I_{BHpred} curve after being fit to the GH_{meas} curve

Step 3: Aggregation and Filtration of Data

In step 2, the procedure for determining the curve (I_{BHpred}) underlying the GH_{meas} plot for the purpose of picking the usable portions of the GH_{meas} curves, was explained. On each of the selected days, after running the solver to determine the curve (I_{BHpred}) underlying GH_{meas}, another macro was run to append the GH_{meas} and I_{BHpred} values pertaining to the 11am to 1pm solar time period into another worksheet called

Estimation_Sheet. In addition, the corresponding values of day of the year, solar time, clock time, air mass ratio and cosine of solar zenith angle were also copied into Estimation_Sheet. Finally, after going through all the selected days, Estimation_Sheet contained data points from all the selected days of 2009. The number of data points totaled 3700. Figure 20 shows a screenshot of the Estimation_Sheet worksheet with day of year, GH_{meas}, cosine of zenith angle, air mass ratio, I_{BHpred}, solar time and clock time of day 1 copied into columns A, B, C, E, F, G and H respectively.

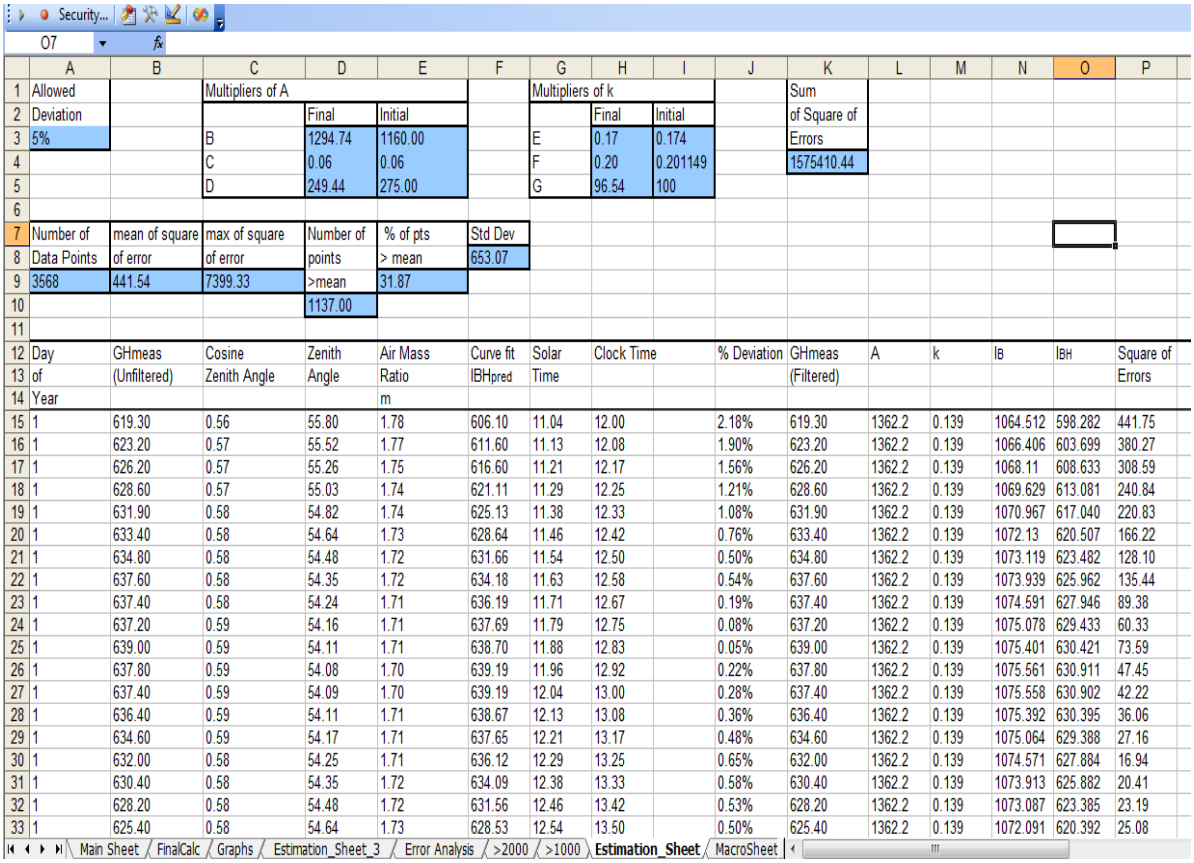

	A	B	C	D	E	F	G	H	I	J	K	L	M	N	O	P
1	Allowed		Multipliers of A				Multipliers of k				Sum					
2	Deviation			Final	Initial			Final	Initial		of Square of					
3	5%		B	1294.74	1160.00		E	0.17	0.174		Errors					
4			C	0.06	0.06		F	0.20	0.201149		1575410.44					
5			D	249.44	275.00		G	96.54	100							
6																
7	Number of	mean of square	max of square	Number of	% of pts	Std Dev										
8	Data Points	of error	of error	points	> mean	653.07										
9	3568	441.54	7399.33	>mean	31.87											
10				1137.00												
11																
12	Day	GHmeas	Cosine	Zenith	Air Mass	Curve fit	Solar	Clock Time		% Deviation	GHmeas	A	k	IB	IBH	Square of
13	of	(Unfiltered)	Zenith Angle	Angle	Ratio	IBHpred	Time				(Filtered)					Errors
14	Year				m											
15	1	619.30	0.56	55.80	1.78	606.10	11.04	12.00		2.18%	619.30	1362.2	0.139	1064.512	598.282	441.75
16	1	623.20	0.57	55.52	1.77	611.60	11.13	12.08		1.90%	623.20	1362.2	0.139	1066.406	603.699	380.27
17	1	626.20	0.57	55.26	1.75	616.60	11.21	12.17		1.56%	626.20	1362.2	0.139	1068.11	608.633	308.59
18	1	628.60	0.57	55.03	1.74	621.11	11.29	12.25		1.21%	628.60	1362.2	0.139	1069.629	613.081	240.84
19	1	631.90	0.58	54.82	1.74	625.13	11.38	12.33		1.08%	631.90	1362.2	0.139	1070.967	617.040	220.83
20	1	633.40	0.58	54.64	1.73	628.64	11.46	12.42		0.76%	633.40	1362.2	0.139	1072.13	620.507	166.22
21	1	634.80	0.58	54.48	1.72	631.66	11.54	12.50		0.50%	634.80	1362.2	0.139	1073.119	623.482	128.10
22	1	637.60	0.58	54.35	1.72	634.18	11.63	12.58		0.54%	637.60	1362.2	0.139	1073.939	625.962	135.44
23	1	637.40	0.58	54.24	1.71	636.19	11.71	12.67		0.19%	637.40	1362.2	0.139	1074.591	627.946	89.38
24	1	637.20	0.59	54.16	1.71	637.69	11.79	12.75		0.08%	637.20	1362.2	0.139	1075.078	629.433	60.33
25	1	639.00	0.59	54.11	1.71	638.70	11.88	12.83		0.05%	639.00	1362.2	0.139	1075.401	630.421	73.59
26	1	637.80	0.59	54.08	1.70	639.19	11.96	12.92		0.22%	637.80	1362.2	0.139	1075.561	630.911	47.45
27	1	637.40	0.59	54.09	1.70	639.19	12.04	13.00		0.28%	637.40	1362.2	0.139	1075.558	630.902	42.22
28	1	636.40	0.59	54.11	1.71	638.67	12.13	13.08		0.36%	636.40	1362.2	0.139	1075.392	630.395	36.06
29	1	634.60	0.59	54.17	1.71	637.65	12.21	13.17		0.48%	634.60	1362.2	0.139	1075.064	629.388	27.16
30	1	632.00	0.58	54.25	1.71	636.12	12.29	13.25		0.65%	632.00	1362.2	0.139	1074.571	627.884	16.94
31	1	630.40	0.58	54.35	1.72	634.09	12.38	13.33		0.58%	630.40	1362.2	0.139	1073.913	625.882	20.41
32	1	628.20	0.58	54.48	1.72	631.56	12.46	13.42		0.53%	628.20	1362.2	0.139	1073.087	623.385	23.19
33	1	625.40	0.58	54.64	1.73	628.53	12.54	13.50		0.50%	625.40	1362.2	0.139	1072.091	620.392	25.08

Main Sheet | FinalCalc | Graphs | Estimation_Sheet_3 | Error Analysis | >2000 | >1000 | Estimation_Sheet | MacroSheet

Fig.20. Screenshot of the spreadsheet (Estimation_Sheet) where data is aggregated and evaluation of new A and k values is performed

In order to pick out the useful portions of the GH_{meas} curve, an upper deviation limit of 5% was set in Estimation_Sheet. All values of GH_{meas} that deviated less than 5% from the underlying curve fit were selected and copied into column K.

To visualize the process of collecting the useful portions of data, consider the GH_{meas} curve of February 06, 2009 before it is filtered (Figure 21). From this curve, portions that deviated less than 5% from the underlying curve (in black) were retained while the other portions were removed. This is illustrated in Figure 22.

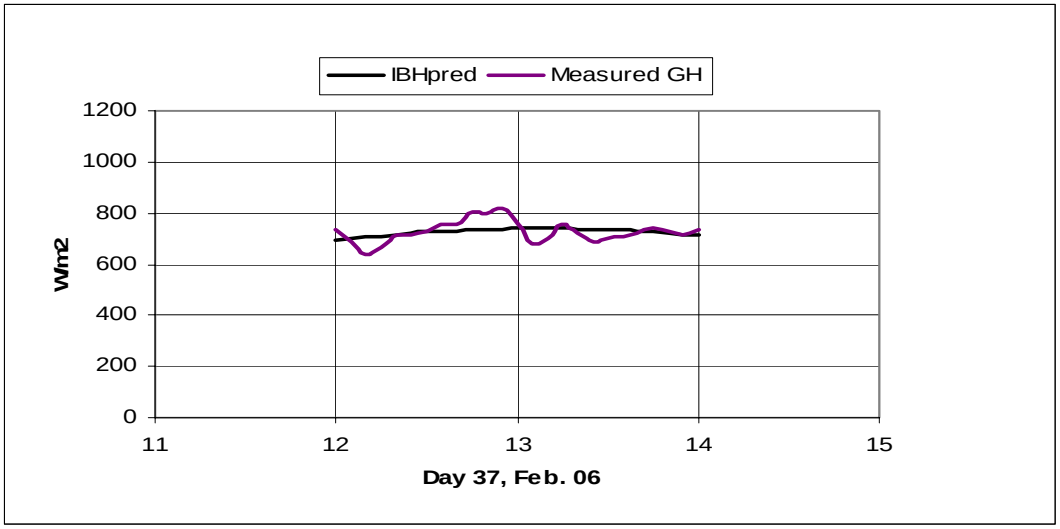

Fig.21. The GH_{meas} curve before portions deviating >5% from underlying black curve were removed

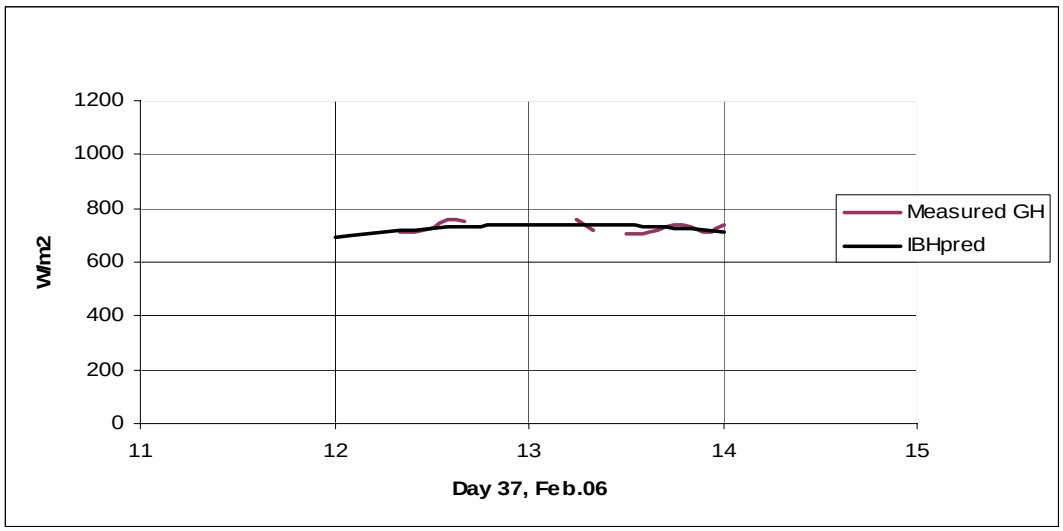

Fig.22. The GH_{meas} curve with portions deviating >5% from underlying black curve removed

Step 4: Estimation of new values of Extraterrestrial Flux Multiplier A and Optical Depth k

The aim of this step was to calculate using the aggregated data, a single set of values of A and k for the whole year – 2009, that when plugged into the equation for I_B would result in an I_{BHpred} that would mimic the GH_{meas} curve. The I_{BHpred} in this case is the final prediction of the beam radiation on a horizontal surface. It is not to be confused with I_{BHpred} calculated in Step 3 (obtained by varying the value of A for every selected day) which was meant purely for the purpose of filtering out deviant data.

The values of A and k in columns L and M of Estimation_Sheet respectively were calculated using:

$$A = B\left\{1 + C\sin\left[\frac{360}{365}(n - D)\right]\right\} \tag{30}$$

$$k = E\left\{1 + F\sin\left[\frac{360}{365}(n - G)\right]\right\} \tag{31}$$

The value of n in the above equations was linked to the corresponding Day of Year cell in column A.

The I_B values of column N were calculated using the equation

$$I_{B=}Ae^{-km} \tag{32}$$

with the values of m, A and k taken from columns E, L and M of the same row. Using the I_B calculated, the I_{BH} values in column O were calculated using

$$I_{BHpred} = I_B \cos\theta_z \tag{33}$$

Column P contained the square of the difference/error between GH_{meas} and I_{BHpred} values. The squares of errors of all the days were summed up and excel solver was used to minimize this sum. This was done in four steps:

1) The values of B, C and D in (30) were initially set to 1160, 0.065 and 275 respectively. These values are got from (8) by writing it in the same form as (30)

2) Similarly, E, F and G in (31) were initially set to 0.174, 0.2011 and 100 respectively with these values derived from (9) written in the same form as (31)

3) Excel solver was run to minimize the sum of squares of errors by varying B, C and D. The new values of B, C and D were found to be 1294.74, 0.0574 and 249.43 respectively

4) With B, C and D set at their new values, excel solver was run again to minimize the sum of squares of errors, but this time varying E, F and G. The new values of E, F and G varied slightly from their initial values, their new values being 0.174, 0.2048 and 96.54 respectively.

Using the newly determined values of the constants, the equations of extraterrestrial flux multiplier A and optical depth k were re-written as:

$$A = 1295\left\{1 + 0.0574\sin\left[\frac{360}{365}(n - 249.43)\right]\right\} \tag{34}$$

$$k = 0.174\left\{1 + 0.2048\sin\left[\frac{360}{365}(n - 96.54)\right]\right\} \tag{35}$$

In addition to calculating the A and k values, the following were also calculated in Estimation_Sheet

- Number of data points left after removing the points deviating >5%
- Mean value of the squares of errors
- Maximum value of the squares of errors
- Number of points with square of error> mean value of squares of errors

Step 5: Error Analysis

By substituting the new values of A and k into the equation for I_B, prediction of I_{BH} was possible. In order to study the accuracy of the prediction, the resulting square of error values from Estimation_Sheet were scatter-plotted vs. Day of the Year. The plot is as shown in Figure 23. Most of the points indicating error >2000 were not evenly distributed during the year but clustered around a few days, specifically days 10, 63, 75, 82, 83, 89, 155, 162 and 190. This can be observed in Figure 23.

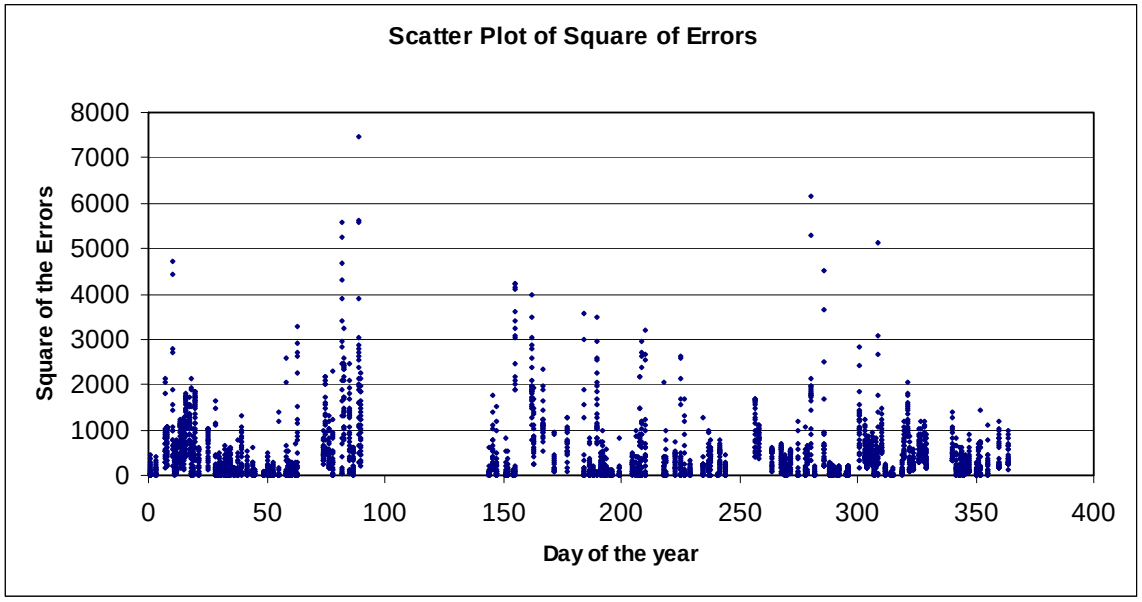

Fig.23: Scatter plot of square of error between GH_{meas} and new I_{BHpred} values

By changing the value of allowed deviation in cell A3 of Estimation_Sheet, the number of data points considered for the estimation of A and k could be varied. The effect of reducing the maximum allowed % deviation between GH_{meas} and I_{BHpred} on the number of data points that are filtered out, the mean square or error and maximum square of error was calculated and studied. The observations are tabulated below in Table 3.

Total Number of Data Points = 3700					
% Deviation allowed	**Number of Data Points After Filtration**	**Mean (of Square of Error)**	**Max (of Square of Error)**	**Number of error points> Mean**	**Std Dev of Square of Error**
<5%	3568	441.54	7399.33	1137	653.07
<4%	3513	425.40	6176.15	1131	607.48
<3%	3417	402.51	6179.68	1112	564.69
<2%	3192	381.27	3998.80	1062	521.46
<1%	2398	339.41	3129.05	795	515.19

Table 3: Effect of reduction of upper % deviation limits between GH_{meas} and I_{BHpred} on error

The important observations from the table 3 are that, as the allowed deviation was tightened: 1) the number of data points available for estimation decreased and 2) the mean and maximum values of square of error decreased.

The values of B, C, D, E, F and G estimated by Estimation_Sheet for each of the % deviation values from Table 3 and tabulated below in Table 4.

% Deviation allowed	**Multiplier of A**			**Multiplier of k**		
	B	**C**	**D**	**E**	**F**	**G**
<5%	1294.743	0.057471	249.4365	0.174162	0.204827	96.54161
<4%	1294.734	0.057597	249.6993	0.174169	0.204619	96.50229
<3%	1295.108	0.05752	249.9958	0.174197	0.204544	96.42696
<2%	1294.928	0.057203	250.1422	0.174245	0.204552	96.27822
<1%	1295.378	0.058277	251.0824	0.174363	0.205123	96.16354

Table 4: Values of B, C, D, E, F and G estimated for different limits of % deviation between GH_{meas} and I_{BHpred}

Step 6: Prediction of Incident Solar Power on Panel

When the measurements of the global and diffuse radiation on a horizontal surface, GH and DH are available, they can be used to calculate the incident solar power incident per unit area of the panel surface can be calculated using the equation [5]:

$$P_{incident} = DH + \frac{(GH-DH)}{\cos\theta_z} \times \cos\theta \ \ (\text{W/ m}^2) \tag{36}$$

In order to predict the solar energy incident on the panel using the GH_{meas} and I_{BHpred} values the following three possibilities were considered:

1) **If** $\boldsymbol{GH_{meas} > |I_{BHpred} + |}$

where I_{BHpred} + is the predicted value of beam radiation plus an upper tolerance of x%. This condition is satisfied when along with a strong beam component of radiation, a diffuse component of radiation is also present.

Therefore, the diffuse horizontal value can be calculated using the equation:

$$DH_{pred} = GH_{meas} - I_{BHpred} \tag{37}$$

From (36) and (37), the solar power incident on the panel surface:

$$P_{pred} = DH_{pred} + \frac{I_{BHpred}}{\cos\theta_z} \times \cos\theta \ \ (\text{W/ m}^2) \tag{38}$$

2) **If** $\boldsymbol{GH_{meas} \approx I_{BHpred}}$

As per (19), the direct normal/beam radiation can be calculated using the following equation:

$$DN_{est} = DH + \frac{(GH - DH)}{\cos\theta_z}$$

On clear sky days, the diffuse horizontal component of radiation is negligible and $GH_{meas} \approx I_{BHpred}$. Therefore, (19) becomes:

$$DN_{est} = \frac{I_{BHpred}}{\cos\theta_z} \tag{39}$$

Using (38), the incident power on the panel surface can be calculated using the following equation:

$$P_{pred} = \frac{I_{BHpred}}{\cos\theta_z} \times \cos\theta \text{ (W/ m}^2\text{)} \quad (40)$$

3) **If** $\boldsymbol{GH_{meas} < |I_{BHpred} - |}$

where I_{BHpred} - is the predicted value of beam radiation minus an lower tolerance of y%. This condition is satisfied when the solar insolation constitutes mainly the diffuse component and the beam component is either absent or weak.

Therefore, under this condition, it can be deduced that the GH_{meas} is made up of mainly the diffuse horizontal component.

$$DH_{pred} = GH_{meas} \quad (41)$$

The solar power incident on the panel surface is,

$$P_{pred} = DH_{pred} = GH_{meas} \text{ (W/ m}^2\text{)} \quad (42)$$

In order to check each of these conditions and calculate the incident power in each case, the following functionalities were included in the main spreadsheet:

- The calculation of I_B and corresponding I_{BH} values using the newly determined values of A and k from step 4.
- The calculation of I_{BHpred} + and I_{BHpred} – values with flexible upper and lower tolerances of x% and y% respectively.
- Determining which of the three conditions were satisfied by the GH_{meas} values: $GH_{meas} > |I_{BHpred} + |$, $GH_{meas} \approx I_{BHpred}$ or $GH_{meas} < |I_{BHpred} - |$ and calculation of P_{pred} using the equation corresponding to each of the conditions – (38), (40) and (42) respectively.
- Calculation of the incident solar power values using the measured values of diffuse and global horizontal radiation:

$$P_{meas} = DH_{meas} + \frac{(GH_{meas} - DH_{meas})}{\cos\theta_z} \times \cos\theta \text{ (W/ m}^2\text{)} \quad (43)$$

Figure 24 shows a screenshot of the part of the spreadsheet that performs the above mentioned calculations.

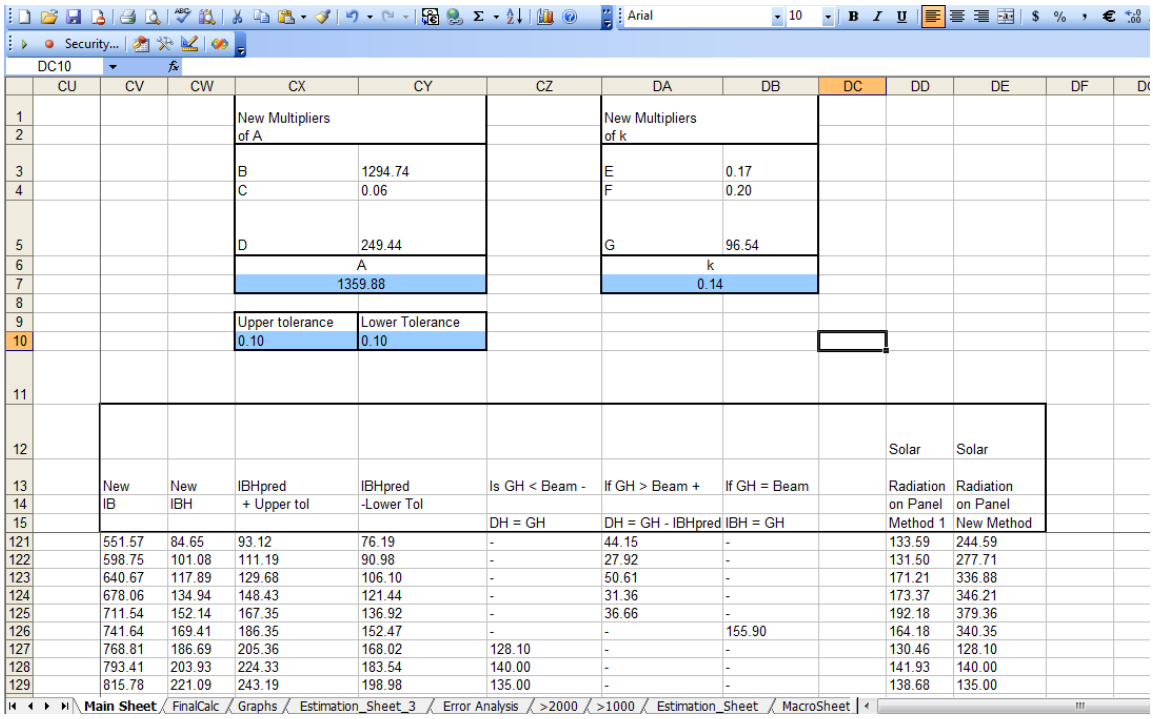

	CU	CV	CW	CX	CY	CZ	DA	DB	DC	DD	DE	DF
1				New Multipliers			New Multipliers					
2				of A			of k					
3				B	1294.74		E	0.17				
4				C	0.06		F	0.20				
5				D	249.44		G	96.54				
6				A			k					
7				1359.88			0.14					
8												
9				Upper tolerance	Lower Tolerance							
10				0.10	0.10							
11												
12										Solar	Solar	
13		New	New	IBHpred	IBHpred	Is GH < Beam -	If GH > Beam +	If GH = Beam		Radiation	Radiation	
14		IB	IBH	+ Upper tol	-Lower Tol					on Panel	on Panel	
15						DH = GH	DH = GH - IBHpred	IBH = GH		Method 1	New Method	
121		551.57	84.65	93.12	76.19	-	44.15	-		133.59	244.59	
122		598.75	101.08	111.19	90.98	-	27.92	-		131.50	277.71	
123		640.67	117.89	129.68	106.10	-	50.61	-		171.21	336.88	
124		678.06	134.94	148.43	121.44	-	31.36	-		173.37	346.21	
125		711.54	152.14	167.35	136.92	-	36.66	-		192.18	379.36	
126		741.64	169.41	186.35	152.47	-	-	155.90		164.18	340.35	
127		768.81	186.69	205.36	168.02	128.10	-	-		130.46	128.10	
128		793.41	203.93	224.33	183.54	140.00	-	-		141.93	140.00	
129		815.78	221.09	243.19	198.98	135.00	-	-		138.68	135.00	

Fig.24. Screenshot showing the calculation of incident power using GH_{meas} *and* I_{BHpred} *values*

Step 7: Model Validation

The model created for the prediction of incident solar power using only measured GH values was validated for the following case:

1) allowed % deviation <5% for data filtration

2) the upper and lower tolerance for the calculation of I_{BHpred} + and I_{BHpred} – each set to 10%.

Figure 24 shows the B, C, D, E, F and G values obtained for the allowed % deviation <5% case from Estimation_Sheet used for the calculation of A and k. It also shows the calculated values of P_{pred} for the different cases of GH_{meas} compared to I_{BHpred} (Column DE) and P_{meas} (Column DD).

The plots of P_{pred} and P_{meas} were plotted onto the same graph in order to compare the closeness of the predicted incident power curve with that obtained using measured values. Figures 25 to 32 show these plots for different days during the year. On some

days such as January 5, 2009 (Figure 25), during the early hours of the morning and late in the evening, when the sun is still low over the horizon, the GH_{meas} curve lies above the I_{BHpred} even though the beam component is negligible. The GH_{meas} curve comprises of mainly the DH component during these hours. However, as per the methodology suggested in Step 6, if $GH_{meas} > I_{BHpred}$ +, (38) will be used for the calculation of P_{pred}. This requires the division of I_{BHpred} by the cosine of the solar zenith angle. During the early hours of the day, since the zenith angle is very high, the cosine of this zenith angle is a very low value. Division of I_{BHpred} by this low value results in a high predicted value of incident power, P_{pred}.

Figures 26 to 32 pertain to plots from summer, spring and winter days. The days cover a range of solar conditions:

a) completely clear sky day (Figure 28),

b) partially clear and cloudy days with portions of high beam and diffuse components (Figures 26, 27, 29, 31 and 32)

c) completely cloudy days with mainly diffuse component (Figure 25)

On each of these days, when a) $GH_{meas} > I_{BHpred}$ + b) $GH_{meas} \approx I_{BHpred}$ and c) $GH_{meas} < I_{BHpred}$ -, equation (38), (40) and (42) respectively were used to calculate the predicted power incident, P_{pred} on the solar panel.

On studying the plots for all the days of the year, it could be observed that the prediction of solar incident power very closely matched the measured values for all hours of the day when the solar zenith angle was lesser than 70^o. During summer and spring, with the sun high up in the sky, the model predicted the incident power for almost the entire daytime. However, during the winter months, with the sun lower in the sky, its zenith angle is $<70^o$ for fewer hours in the day and the model could be used accurately for those hours only.

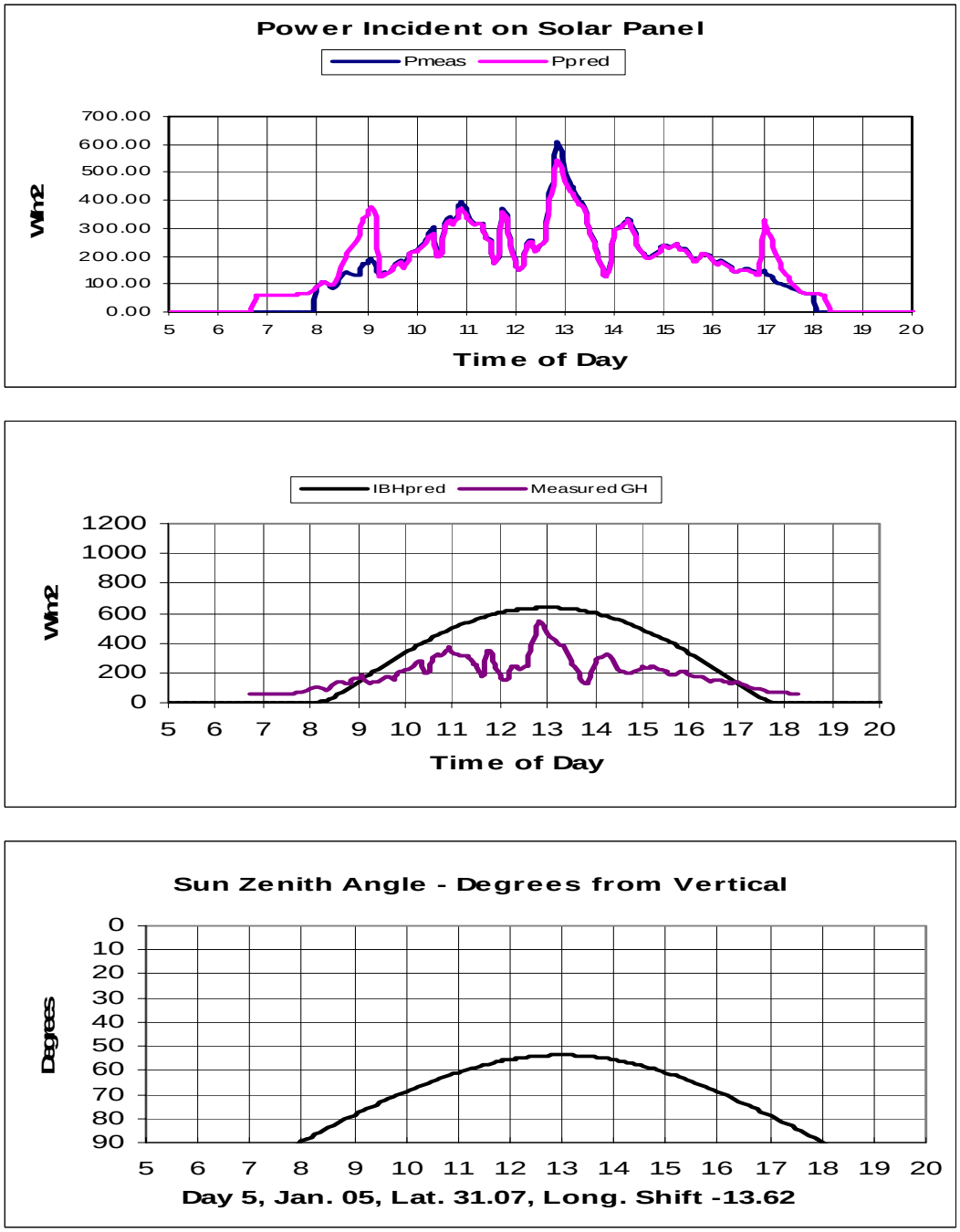

Fig.25. Curves of a) P_{pred} and P_{meas}, b) I_{BHpred} and GH_{meas} and c) solar zenith angle from top to bottom on January 5, 2009. Between 9am and 5pm clock time, $GH_{meas} < I_{BHpred}$ -. In this case, condition 3 is satisfied

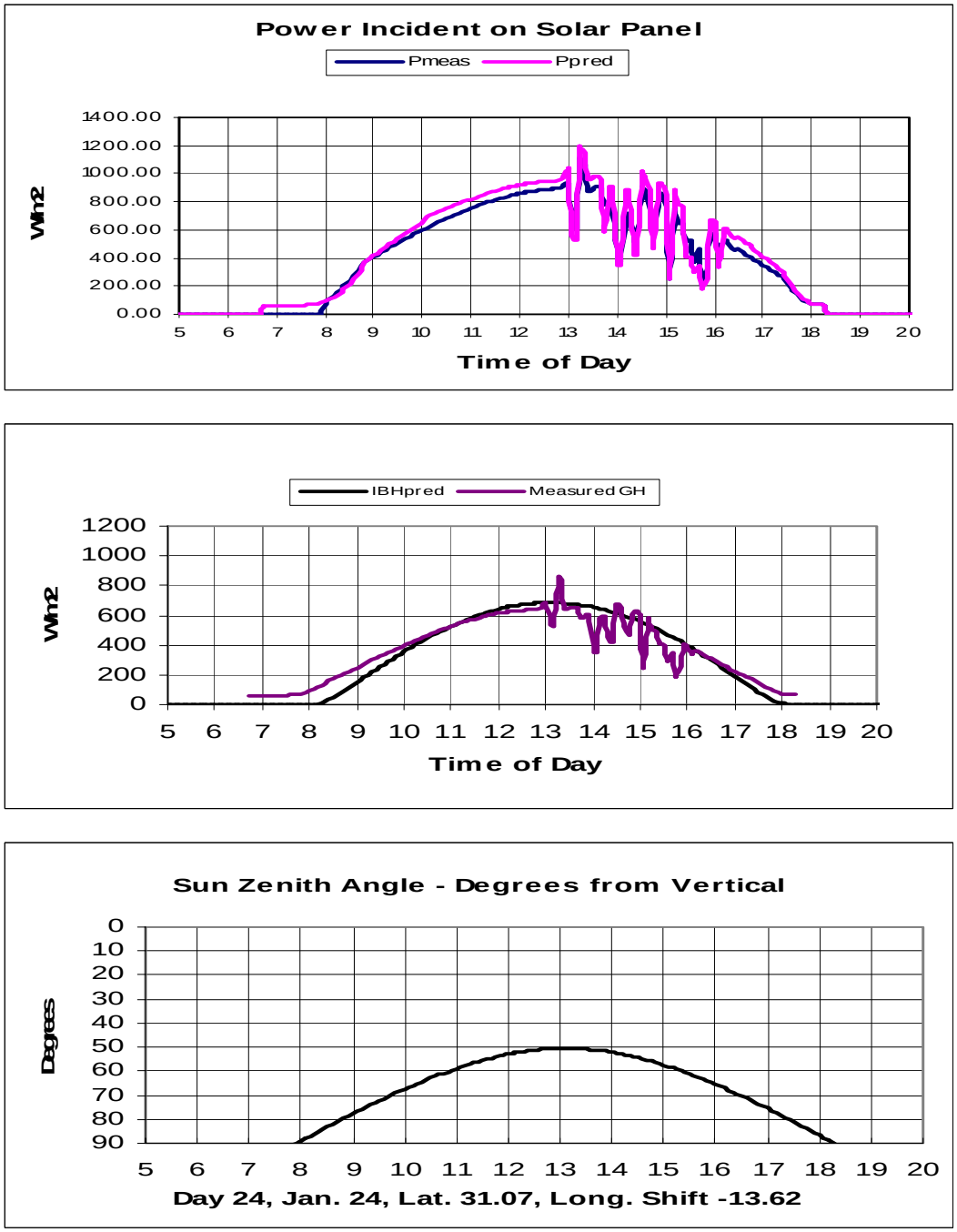

Fig.26. Curves of a) P_{pred} and P_{meas}, b) I_{BHpred} and GH_{meas} and c) solar zenith angle from top to bottom on January 24, 2009

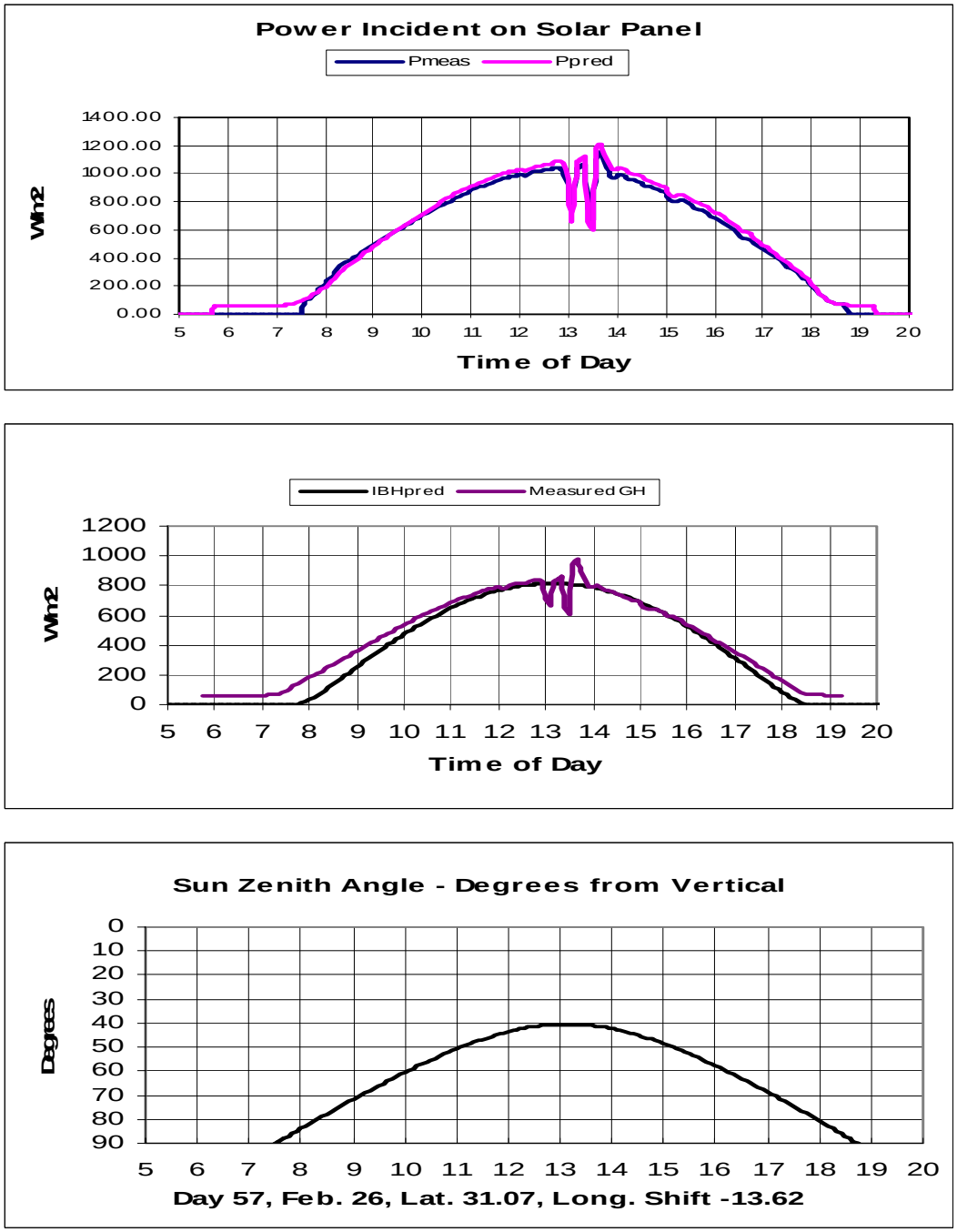

Fig.27. Curves of a) P_{pred} and P_{meas}, b I_{BHpred} and GH_{meas} and c) solar zenith angle from top to bottom on February 26, 2009

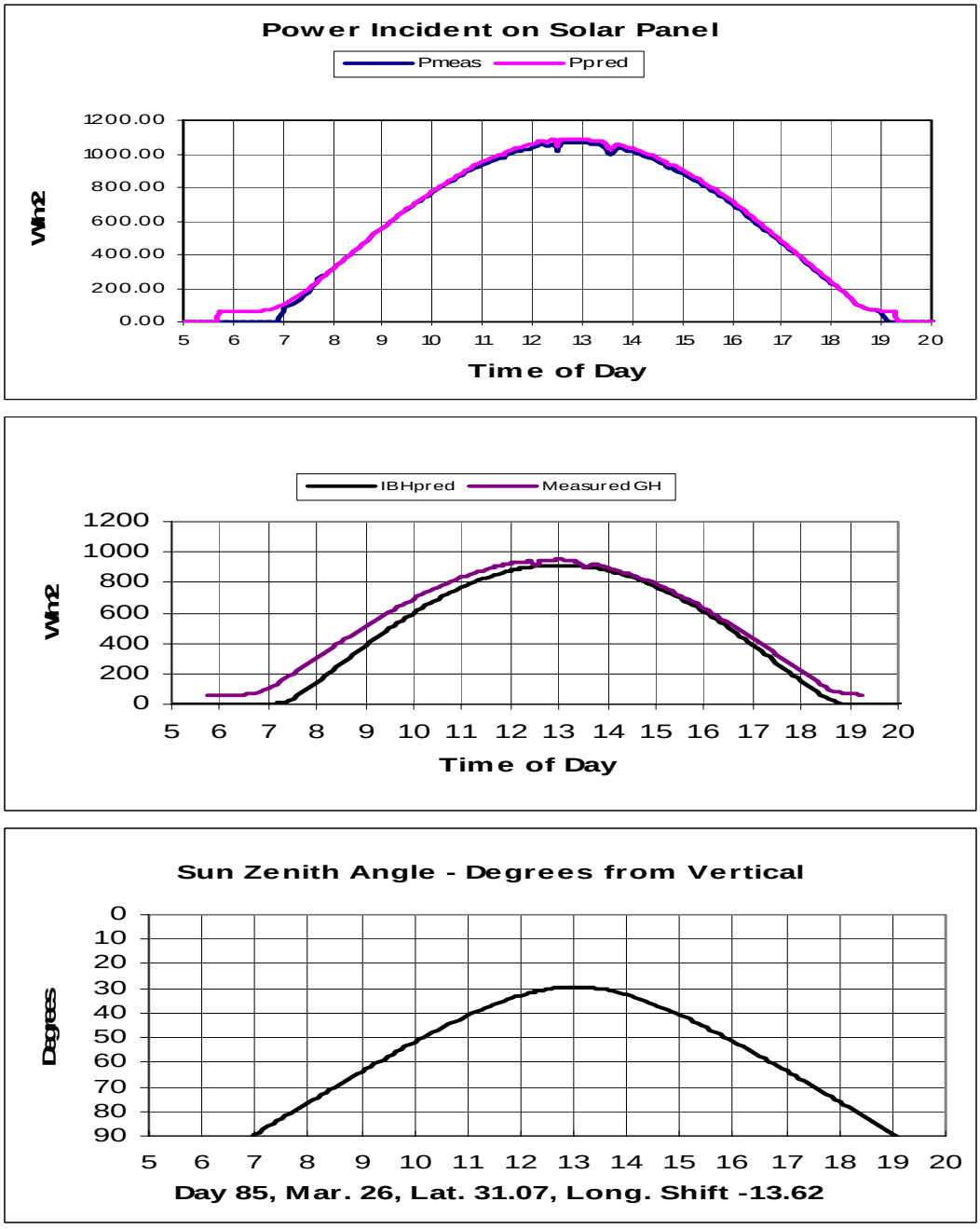

Fig.28. Curves of a) P_{pred} and P_{meas}, b) I_{BHpred} and GH_{meas} and c) solar zenith angle from top to bottom on March 26, 2009

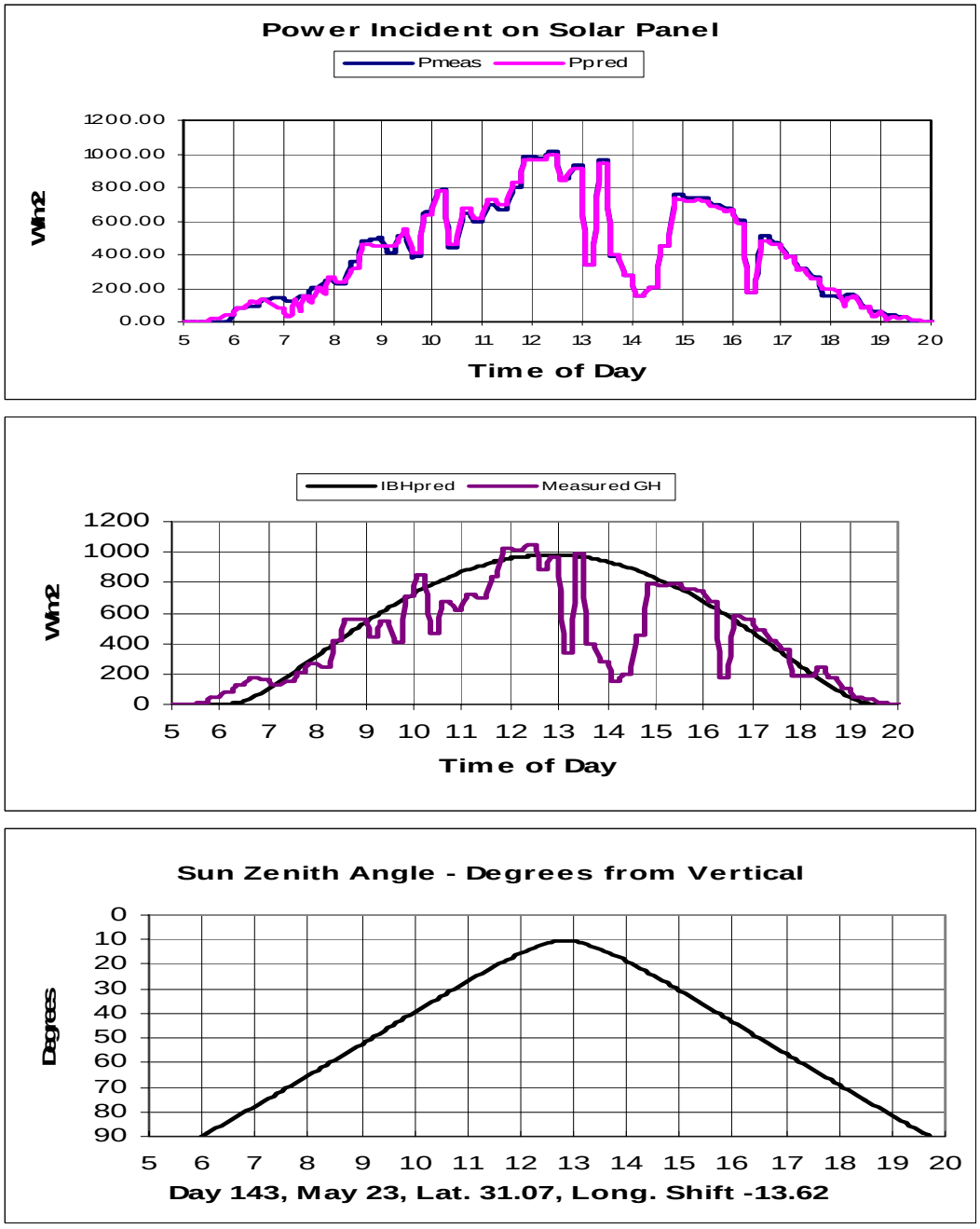

Fig.29. Curves of a) P_{pred} and P_{meas}, b) IBHpred and GH_{meas} and c) solar zenith angle from top to bottom on May 24, 2009

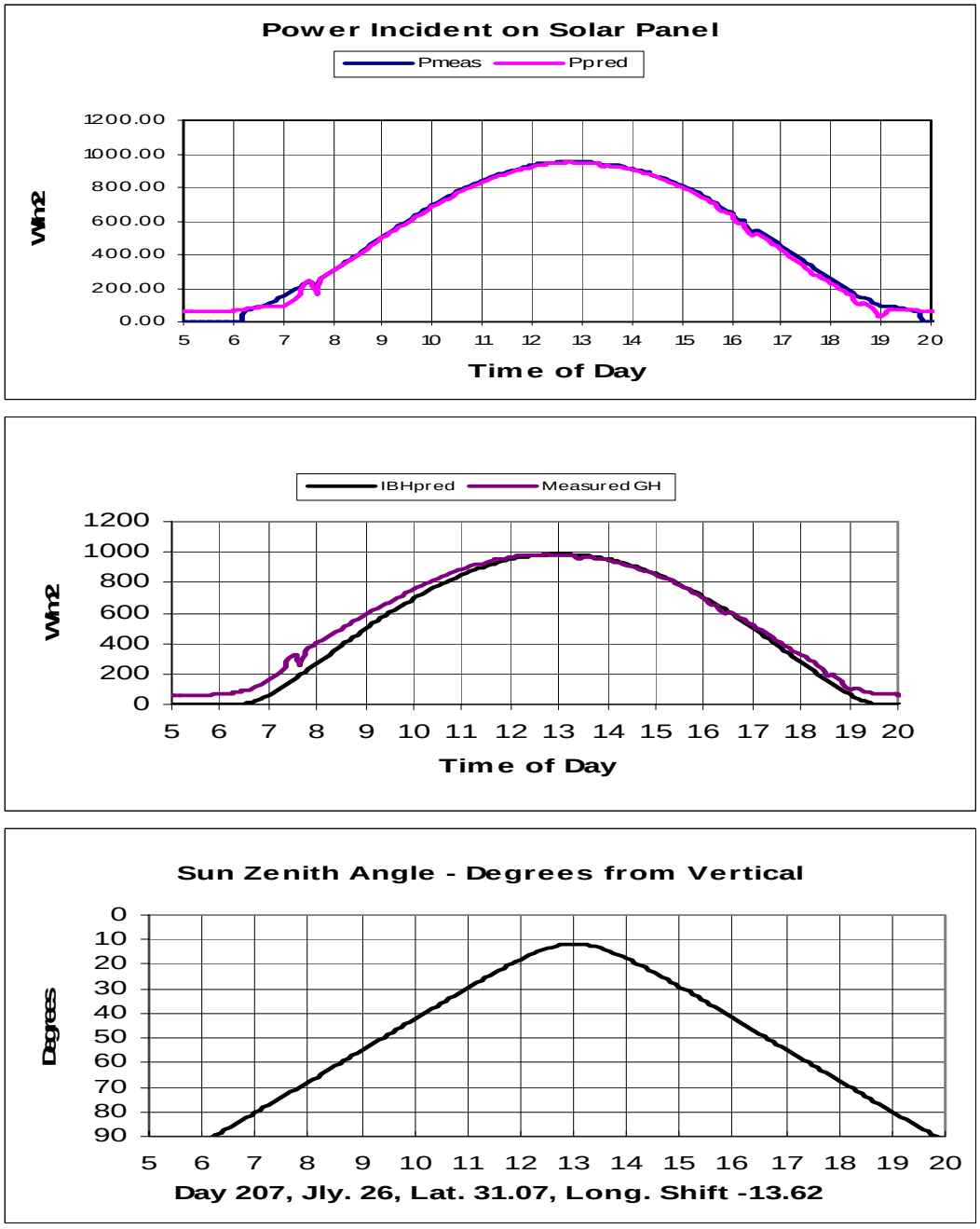

Fig.30. Curves of a) P_{pred} and P_{meas}, b) I_{BHpred} and GH_{meas} and c) solar zenith angle from top to bottom on July 26, 2009

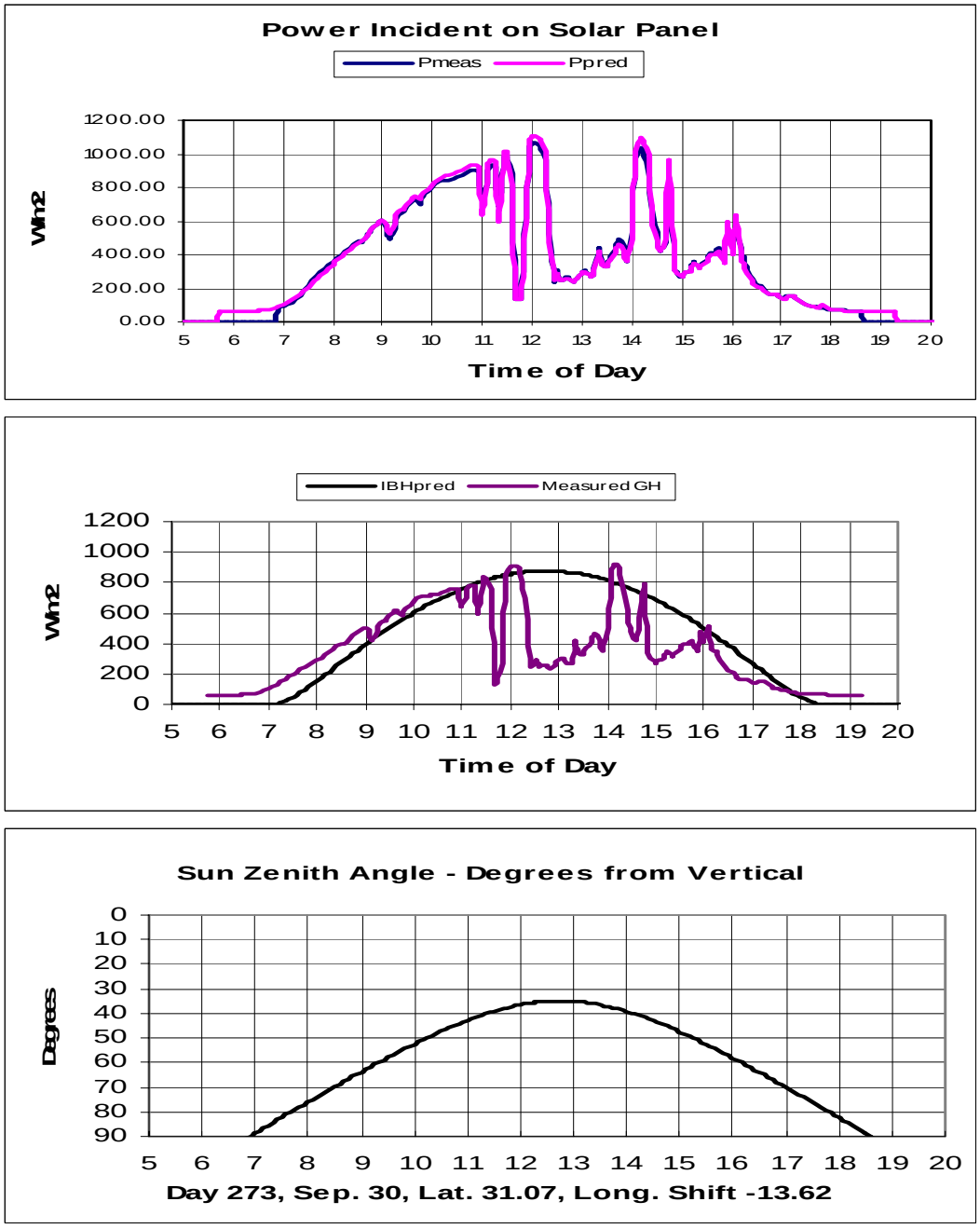

Fig.31. Curves of a) P_{pred} and P_{meas}, b) I_{BHpred} and GH_{meas} and c) solar zenith angle from top to bottom on September 30, 2009

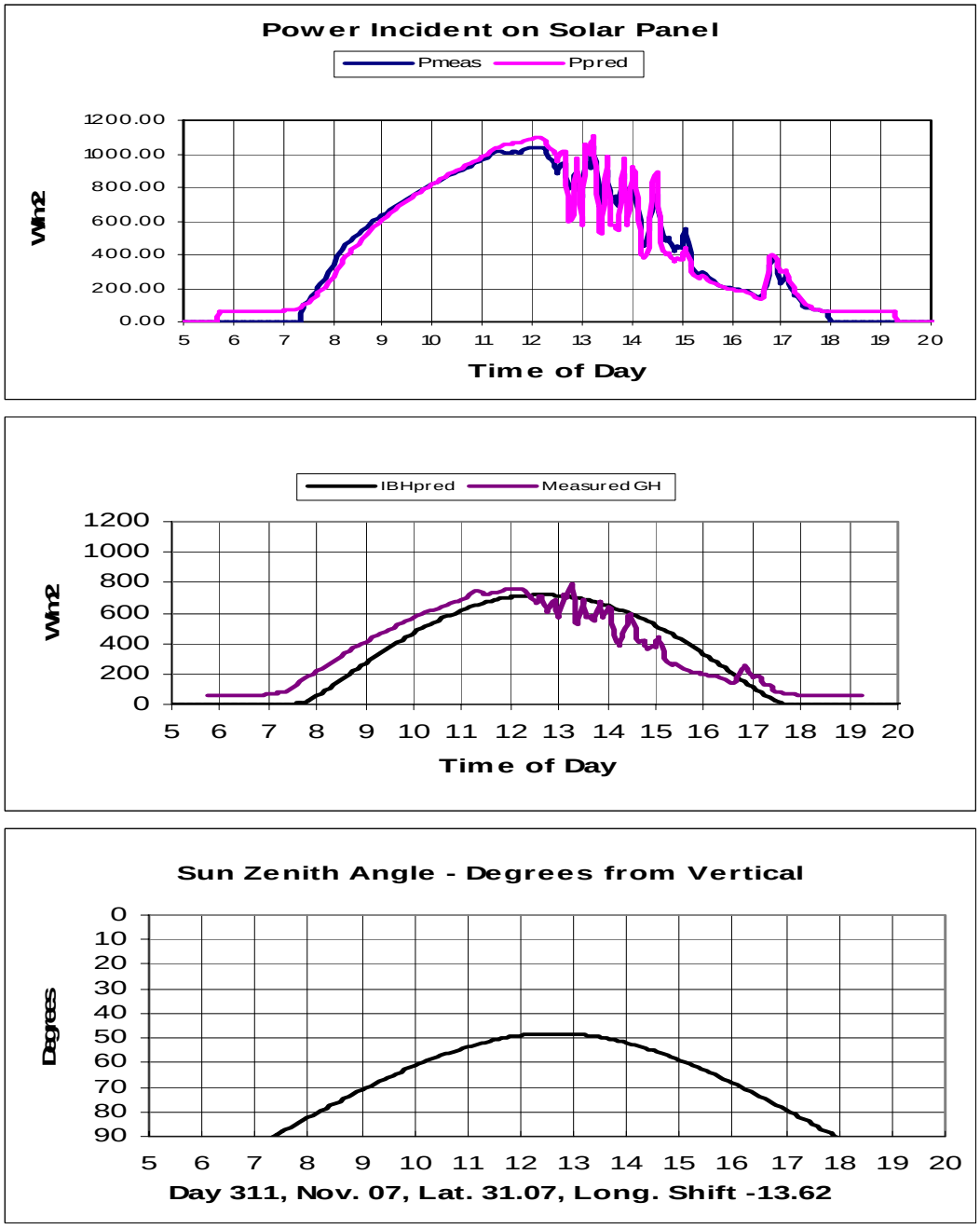

Fig.32. Curves of a) P_{pred} and P_{meas}, b) IBHpred and GH_{meas} and c) solar zenith angle from top to bottom on November 07, 2009

On each of the days illustrated in Figures 25 to 32, the measured and predicted solar energy incident on the panel, E_{meas} and E_{pred} respectively, were calculated for solar zenith angles < 70^o using the following equations:

$$E_{meas} = \frac{\sum P_{meas}}{12\times1000} \text{ kWh/ m}^2 \quad (44)$$

$$E_{pred} = \frac{\sum P_{pred}}{12\times1000} \text{ kWh/ m}^2 \quad (45)$$

where P_{meas} and P_{pred} are calculated using equations presented earlier. The division by 12 was to account for the fact that GH_{meas} and I_{BHpred} values pertain to 5 minute intervals and an hour is made of 12 such intervals. Table 5 shows the E_{pred} and E_{meas} values obtained. It can be observed from Table 5 that the predicted values of incident solar energy very closely matched the measured values. If the efficiency η, of the solar conversion device was known, the energy output of the device could be calculated simply by multiplying E_{pred} with η.

Day of Year	**E_{meas} (kWh/m^2)**	**E_{pred} (kWh/m^2)**	**% error between E_{meas} and E_{pred}**
5-Jan-09	1.728	1.674	3%
24-Jan-09	4.783	5.090	6%
26-Feb-09	6.586	6.834	4%
26-Mar-09	7.390	7.536	2%
24-May-09	7.135	7.094	1%
26-Jul-09	7.150	7.032	2%
30-Sep-09	4.739	4.771	1%
7-Nov-09	5.181	5.139	1%

Table 5: Measured and predicted values of solar energy incident on collector on different days of the year

Chapter 8

Conclusion

The knowledge from an existing solar radiation estimation model and observations from the analysis of existing solar radiation data measurements were used to develop a methodology to aid in the prediction of incident power on a solar panel. A set of new equations were developed to predict the beam radiation on a horizontal surface. By making a few approximations, utilizing only the global horizontal radiation measurements and beam radiation predictions, the incident solar power on the collector was forecasted. The predicted values of power were compared with the measured values on days with different sky conditions for the purpose of validation. For the location where the data was collected (West Texas), it was found that for all hours of the day when solar zenith angle is lesser than 70^{o}, the model predicted the incident solar power correctly.

The model presented in this thesis can be used to accurately predict the solar power/energy incident on a collector at any location possessing global horizontal radiation measurements simply by recalculating the multipliers of extraterrestrial flux multiplier and optical depth using the equations and methodology put forth in this thesis. If the efficiency of the solar energy conversion device is known, the energy output from it can be predicted.

Bibliography

[1] http://solar-is-future.com

[2] National Renewable Energy Laboratory-Solar Radiation Resource Assessment Project. Shining *On – A Primer on Solar Radiation Data*. May,1992.

[3] G. M. Masters. *Renewable and Efficient Electric Power Systems*. New Jersey: Wiley Interscience. 2004. p. 407-446.

[4] http://rredc.nrel.gov/solar/glossary/

[5] W. Mack Grady. Class Lecture. Department of Electrical and Computer Engineering, EE362L: *Power Electronics, Solar Power, I-V characteristics.* University of Texas at Austin. Fall 2008.

Vita

Niveditha Hanumantha Reddy was born in Bangalore, India. She studied Electrical and Electronics Engineering at B.M.S College of Engineering, Bangalore (affiliated to Visveswaraiah Technological University) and received the Bachelor of Engineering Degree in June, 2007. During the following year she was employed as a software developer for IBM, Global Business Services, India. In August, 2008, she entered the Graduate School at The University of Texas at Austin.

Email: reddy.niv@gmail.com

This thesis was typed by the author.